Two-pion Production and Isovector Double-Pionic Fusion : The pp$\rightarrow$ pn$\pi^+\pi^0$ and pp $\rightarrow$ d$\pi^+\pi^0$ Reactions

Dissertation
zur Erlangung des Grades eines
Doktors der Naturwissenschaften
der Fakultät für Mathematik und Physik
der Eberhard-Karls-Universität Tübingen

vorgelegt von
Florian Kren
aus Esslingen

Tübingen

2010

Tag der mündlichen Prüfung:	02.07.2010
Dekan:	Prof. Dr. Wolfgang Knapp
1. Berichterstatter:	Prof. Dr. Heinz Clement
2. Berichterstatter:	Prof. Dr. Gerhard J. Wagner

Abstract

For long two-pion production has been a subject of interest, especially since the ABC effect was observed, which is an unexpected enhancement in the momentum spectrum of fused nuclei. The first measurements were inclusive, i.e. measured only the outgoing fused nucleus. As in inclusive measurements $\pi\pi$ production can be admixed with three-pion production and products from other reaction channels, a comprehensive research program was started at the CELSIUS/WASA facility to carry out exclusive measurements for many different pion production processes.
The WASA detector covers nearly the full solid angle of 4π. With good detection capabilities for charged and neutral particles in the central part and very good identification of charged particles in the forward part, the WASA detector is well suited for exclusive measurements of this type of reactions.
The ABC effect has been interpreted as a t-channel $\Delta\Delta$ excitation in the course of the reaction process. The calculations predict a peak at low and at high invariant mass in the invariant mass spectrum of $\pi\pi$. But the new exclusive measurements show, that the ABC effect is an isoscalar enhancement only at low invariant $\pi\pi$ mass - no high invariant mass peak - correlated with a narrow resonance-like structure in the total cross section.
To test this conclusion and to study a clean example of t-channel $\Delta\Delta$ excitation without ABC effect exclusive measurements of the isovector reaction $pp \rightarrow d\pi^+\pi^0$ have been carried out at T_p = 1.1 GeV. Additionally the reaction $pp \rightarrow pn\pi^+\pi^0$ was measured, in order to see the difference between fusion and non-fusion processes.
The measurements show that the $pp \rightarrow d\pi^+\pi^0$ channel exhibits no enhancement at low invariant masses, meaning no ABC effect. This is expected from an isovector channel due to the fact, that the pion pair must be in relative p-wave, which suppresses any enhancement at low invariant masses. Therefore this most basic isovector double-pionic fusion reaction qualifies as an ideal test case for the conventional t-channel $\Delta\Delta$ excitation process. Indeed, the obtained differential distributions reveal the conventional t-channel $\Delta\Delta$ mechanism as the appropriate reaction process, which also accounts for the observed energy dependence of the total cross section.
These results have been published in Physics Letters B 684 (2010) 110-113.
Although no good description of the reaction mechanism for $pp \rightarrow pn\pi^+\pi^0$ is available, the differential cross sections confirm the presence of very different reaction processes in the fusion and the non-fusion channel, respectively.

Contents

1. Introduction

The study of double-pionic fusion is a subject of interest, since 50 years ago an unexpected effect was observed by Abashian, Booth and Crowe, the so-called ABC effect (Ref. [1]). The studied reactions were of the form

pp or pn or pd $\rightarrow$ fused nucleus + X ,

where X stands for unobserved reaction products. In such inclusive measurements only the fused nucleus was detected using a single arm magnetic spectrometer. Later experiments confirmed (Ref. [2]-[5]), that the ABC effect is only present when a bound nuclear system is formed.

The ABC effect shows up as an unexpected enhancement in the momentum spectrum of the nucleus, see figure 1.1.

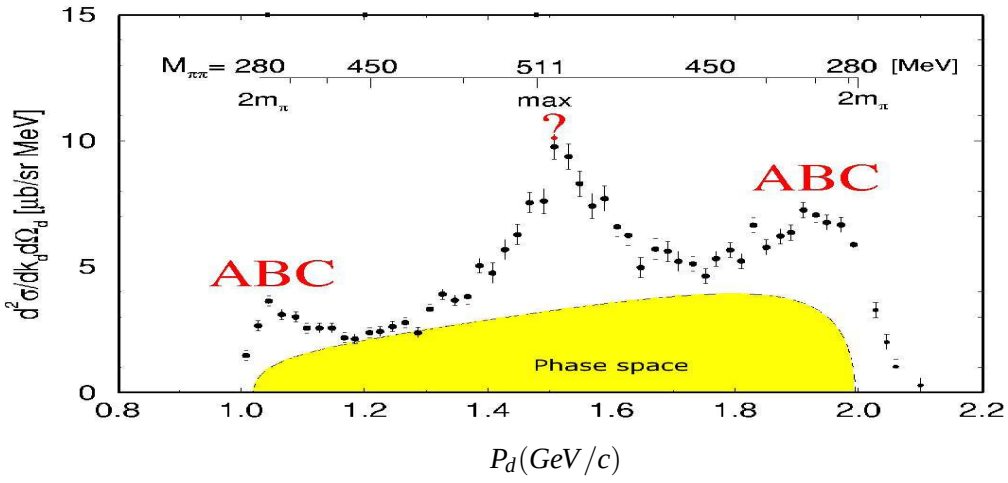

Figure 1.1.: Deuteron momentum with P_{beam} = 1.88 GeV/c. Black data points from Plouin et al. (Ref. [4]), yellow area is phase space in case of $\pi\pi$-production and upper scale translates the deuteron momentum into invariant mass of $\pi\pi$

The invariant mass of a particle set j is defined as:

$$M^2 = (\sum_j E_j)^2 - (\sum_j p_j)^2 (c = 1)$$

where E denotes the total energy of particle j and p the momentum of particle j. In case the relative momentum of the particles j is small, the invariant mass is small. In case the relative momentum is large, the invariant mass is large.

In case of reaction products nucleus + X, a high nucleus momentum in the possible kinematical range means, that due to energy conservation X can have only little total energy and therefore the particles making up X can only have a small relative momentum. A low nucleus momentum means, that due to momentum conservation X needs to have a large momentum along beam axis and therefore the X particles can have only little relative momentum.

Therefore the peaks at low and high momenta in Figure 1.1 reflect a peak at low invariant masses in the invariant mass spectrum of X. In case of a momentum of the nucleus in the middle of the possible range, the relative momentum of the X particles is less limited. The peak in the middle of the possible range of the nucleus momentum is correlated with a high invariant mass peak in the invariant mass spectrum of X. As indicated by the upper scale in Figure 1.1 this correlation is non-linear.

Assuming X to be two pions ($\pi\pi$) and translated into the invariant mass of the $\pi\pi$-system (upper scale in Figure 1.1), this means that there is an enhancement at low and high $\pi\pi$ invariant masses. Since the invariant mass of two particles is correlated with the relative momentum of the particles, the $\pi\pi$ would tend to move either in parallel or antiparallel. The ABC effect was only found in scalar-isoscalar channels (Ref. [1], [2], [3]).

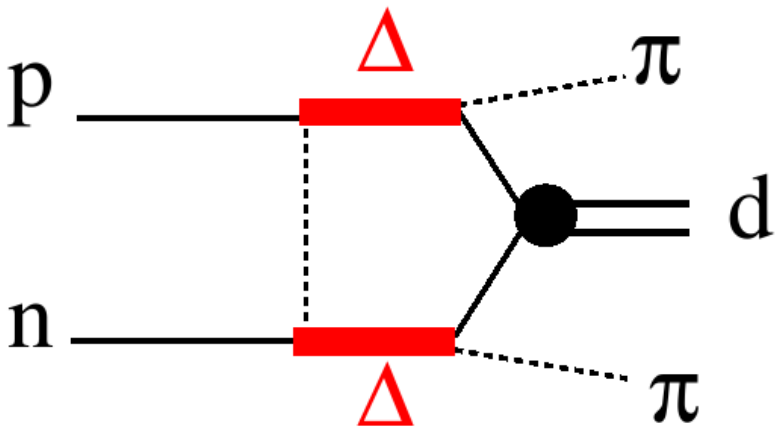

Figure 1.2.: Double-pionic fusion process via t-channel $\Delta\Delta$ excitation in the intermediate state for the reaction $pn \rightarrow d\pi^+\pi^0$

It has been interpreted as a t-channel ΔΔ excitation (Ref. [6], [7]). Fig. 1.2 shows the corresponding graph. A pion exchange leads to the formation of two Δs - mass 1.232 GeV each - which then decay both into nucleon and pion. The two nucleons then fuse and form a deuteron.

Such an excitation would produce an enhancement at low and high ππ invariant mass.

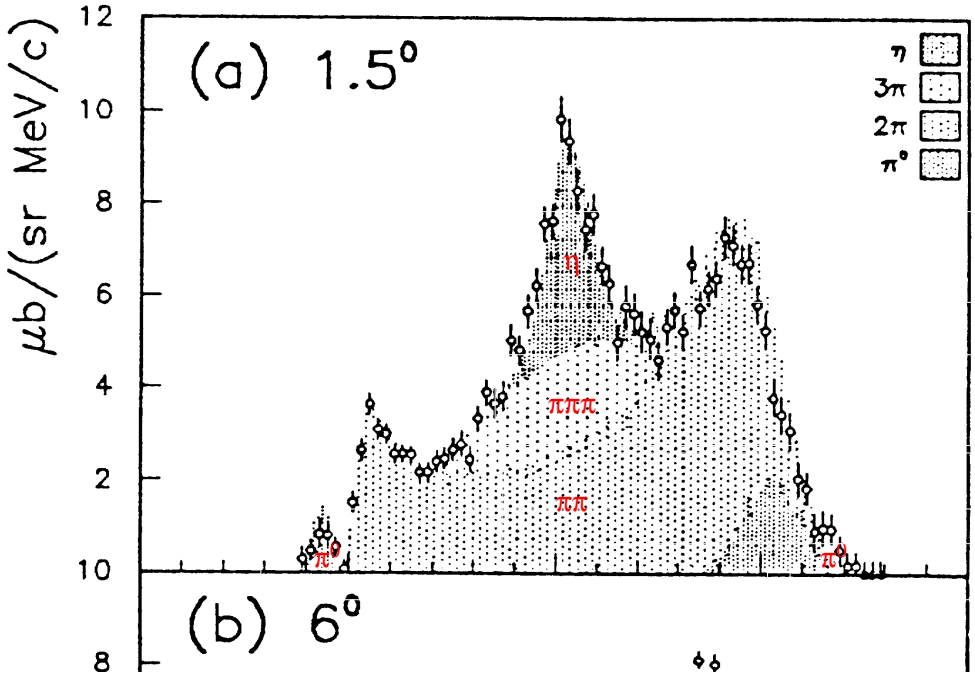

Figure 1.3.: Interpretation of the data from Plouin et al. (Ref. [4]) by Plouin, Fleury and Wilkin (Ref. [5])

But as these first experiments observing the ABC effect were inclusive, measuring only the outgoing nucleus, it was unknown, whether the X are truly ππ or something else. As demonstrated in Ref. [5] identifying the middle bump in the momentum spectra as a high invariant mass peak of ππ-system could be a mistake as X could also be 3 π or eta, see figure 1.3.

Inclusive measurements cannot decide this issue and the only exclusive measurements at that time with energies near the double Δ energy region were low statistics bubble chamber measurements (Ref. [8], [9]).

Therefore exclusive measurements were carried out at CELSIUS-WASA and WASA@COSY for the reactions $pn \rightarrow d\pi^0\pi^0$, $pd \rightarrow {}^3He\pi\pi$ and $dd \rightarrow {}^4He\pi\pi$ (Ref. [10]-[15]) . The high invariant mass peak in $M_{\pi\pi}$ is not visible in exclusive measurements - in the inclusive measurements it had been caused by η and 3 π production - , whereas the low invariant mass peak is very pronounced. Therefore the pions tend to have a low relative momentum. Since they emerge from two different Δs,which are formed at or even below the nominal ΔΔ threshold, this suggests, that the two Δs have a low relative momentum towards each other. Hence a final state interaction or even binding between the two Δs was proposed. Calculations based on this describe the data of the different reactions measured at WASA very well (Ref. [19]). New measurements (Ref.

[11]-[13], [15]) show that the ABC effect is correlated with a resonance-like structure in the total cross section, which constitutes the first evidence for a resonance in the baryon-baryon system.

Since such a big step in understanding the ABC effect happened by measuring exclusively instead of inclusively, it was decided to measure also an isovector channel exclusively in order to study a clean $\Delta\Delta$ reaction and to see whether the ABC effect is indeed restricted to the scalar-isoscalar double-pion production. So far only inclusive (Ref. [1], [2]) or low-statistic bubble chamber data (Ref. [8], [9]), lacking information on differential observables, exist. Data taken at CELSIUS/WASA in May 2003 were analysed for the $pp \to d\pi^+\pi^0$ reaction channel. The results are presented in this work.

At CELSIUS-WASA non-fusion double-pionic reactions were also studied (Ref. [16]). As expected they show no distinctive sign of ABC effect. In these channels the Roper excitation is present in addition to the t-channel $\Delta\Delta$ excitation. According to the calculations shown in Ref. [21] and [16] the Roper decays dominantly into $N(\pi\pi)_{I=0}$. The protons have isospin of 1/2, the left side of $pp \to d\pi^+\pi^0$ has isospin 1. Deuteron has isospin 0, therefore $\pi^+\pi^0$ has isospin 1 and not isospin 0 as preferred in Roper excitation. As a consequence the Roper is suppressed and the $pp \to d\pi^+\pi^0$ channel allows a rather clean study of the double Δ process as also there is no ABC effect .

As the two pions have isospin one, their wave functions are antisymmetric in the isospin part. Due to Bose symmetry their wave function has to be symmetric. This requirement forces the pions to be antisymmetric in angular momentum, as their spin is zero and therefore symmetric. Therefore they are expected to have odd relative angular momentum, most likely l=1. These quantum numbers would fit a ρ, therefore it is possible, that the two pions form a ρ in an intermediate state.

In order to have a comparison of double-pionic production with and without fusion of the nucleus, the same May 2003 data were analysed also for the $pp \to pn\pi^+\pi^0$ channel.

2. Experimental Setup

2.1. Theodor Svedberg Laboratory (TSL)

The experiment took place at the Theodor Svedberg Laboratory in Uppsala. The measurements were done with the WASA detector, which was an internal detector in the CELSIUS accelerator and cooler storage ring. The Gustaf Werner Cyclotron accelerated the particles initially, then the beam was injected into CELSIUS.

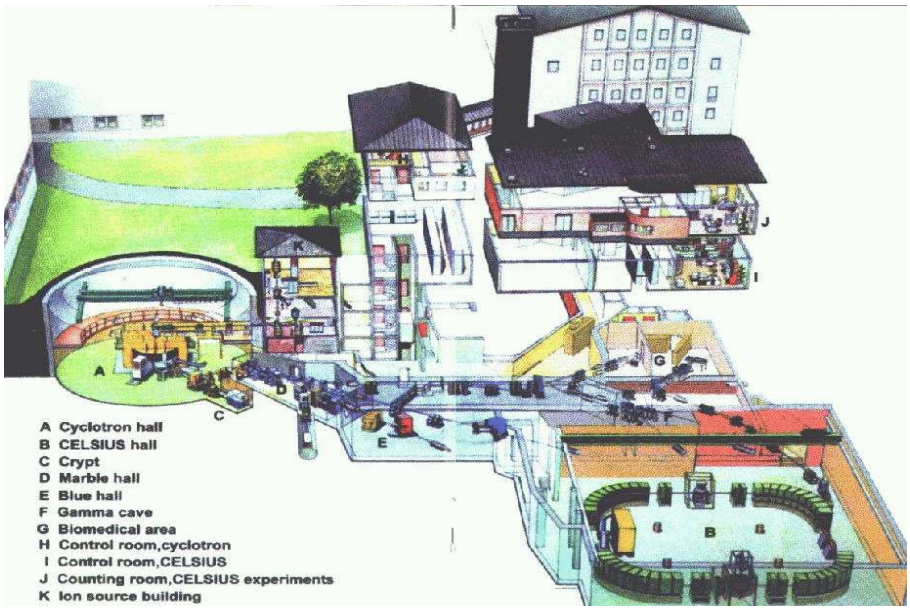

Figure 2.1.: Theodor Svedberg Laboratory (TSL) from Ref. [12]

2.2. CELSIUS

CELSIUS is a abbreviation for Cooling with ELectrons and Storing Ions from Uppsala Synchrocyclotron. It had in total 40 dipole (green rectangles in Fig. 2.2) and 8 quadrupole magnets (blue rectangles in Fig. 2.2) in the curved sections. The 4 straight sections contained the injection, the electron cooler, a cluster jet target and the pellet target of the WASA detector. CELSIUS was operated in cycles, each one about 2 - 3 minutes long. A cycle consisted of beam injection, acceleration, flat top, deceleration, beam dumping and readying the magnets for the next injection. In the acceleration phase the beam energy was increased to the intended value and in the

following flat top it was kept stable for data taking.

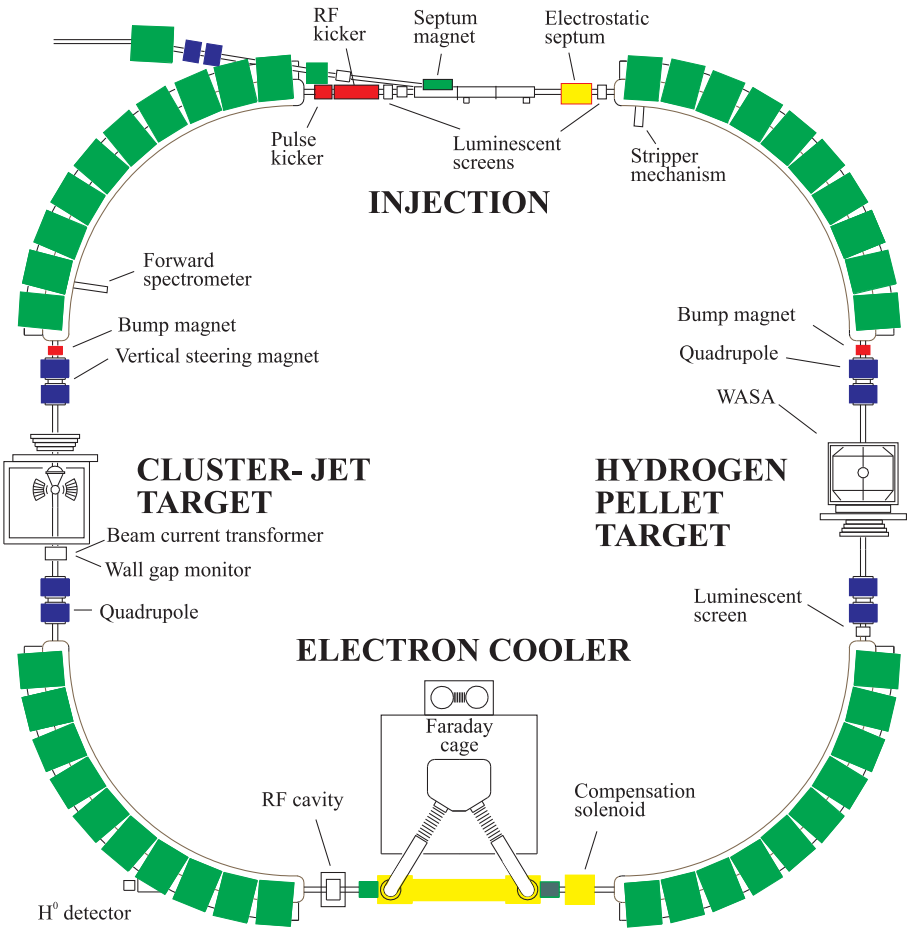

Figure 2.2.: CELSIUS from Ref. [12]

2.3. WASA detector

The Wide Angle Shower Apparatus (WASA) is a 4π (4π stands here for full solid angle) detector, which was designed to measure the production of light mesons. The detector (Fig. 2.3 and 2.4) is made up of 4 parts, pellet target, Central Detector, Forward Detector and zero degree spectrometer. The zero degree spectrometer allows measurement of heavy hadrons, which due to the reaction kinematics move close to the beam axis. The reaction studied in this work does not have such reaction products, therefore the zero degree spectrometer is not described in detail. The detector has two distinctive parts, because WASA was designed to exclusively measure both neutral and charged mesons and their decay products and hadrons. Light mesons and their decay products are best detected with a high Z material, whereas for the charged heavy hadrons low Z material is best to reduce hadronic interactions.

Due to kinematics the heavy hadrons tend to go in forward direction, therefore the Forward Detector uses low Z materials and is optimized to measure protons and other charged hadrons. It also has some limited neutron detection capability.

Light mesons and especially their decay products can go in any direction, therefore the Central Detector covers a large angle and uses high Z material for detection. To distinguish differently charged mesons a magnetic field is used.

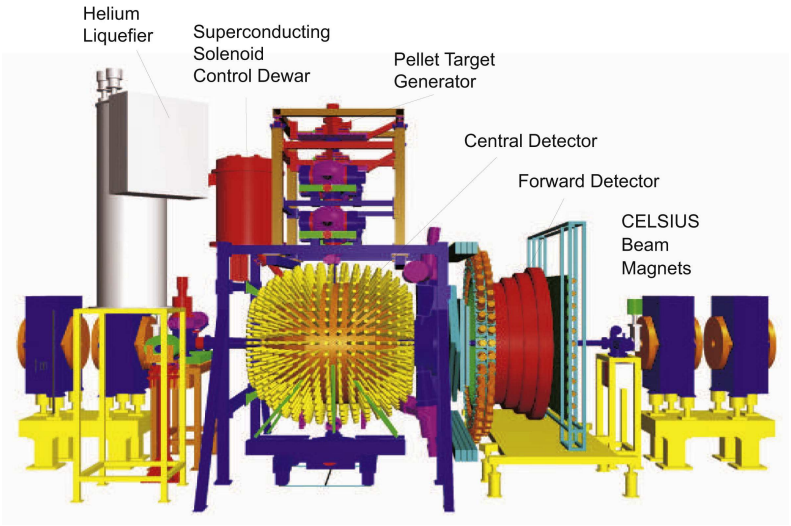

Figure 2.3.: CAD view of WASA detector from Ref. [17]

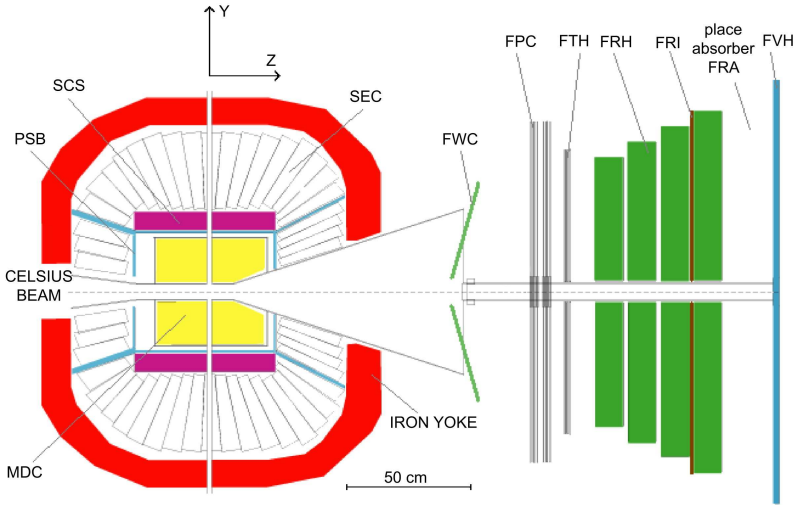

Figure 2.4.: Cross section view of WASA detector from Ref. [17]

2.3.1. Pellet target

The pellet target system (Fig. 2.5) provides an internal target for the beam. First a gas - hydrogen in our case - is liquified. A jet of the liquified gas is then shot through a thin vibrating nozzle, which causes the jet to break up into droplets. The droplets freeze by vacuum evaporation and then form a beam of pellets. The pellets pass through a long thin pipe into the scattering chamber. Since the pipe is long and thin, it occupies not much space, which is a necessity for the setup of the WASA 4π detector. In the scattering chamber the pellets cross the beam pipe and fall into the pellet beam dump. This setup effectively provides a point like target and does not reduce the circulating beam intensity too fast, see Table 2.1 for pellet jet properties.

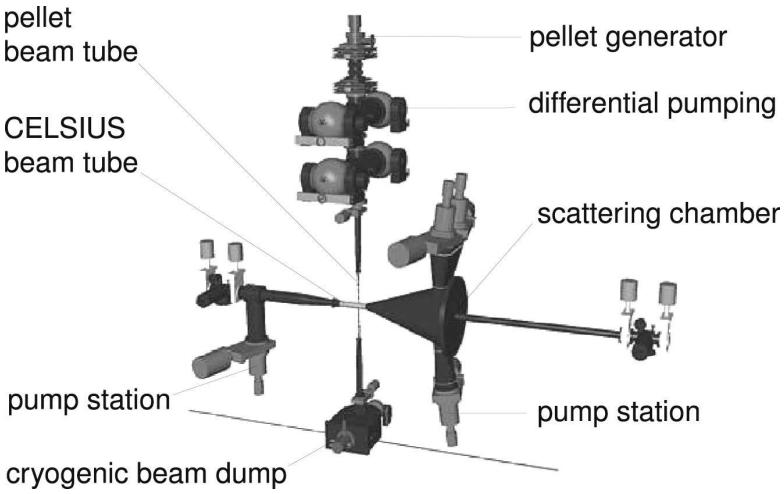

Figure 2.5.: Pellet target system from Ref. [17]

Pellet diameter (μm)	25-35
Pellet frequency (kHz)	5-12
Pellet-pellet distance (mm)	9-20
Effective target area density (at/cm^2)	$>$1015
Beam diameter (mm)	2-4

Table 2.1.: Pellet target properties

2.3.2. Central Detector (CD)

The Central Detector consists of 3 different detectors and the Superconducting Solenoid (SCS) for creating a magnetic field. Closest to target is the Mini Drift Chamber (MDC). The magnetic field causes charged tracks to have a curvature. This curvature is measured by MDC, which allows to gain momentum information.

Surrounding the MDC and in front of the SCS there is the Plastic Scintillator Barrel (PSB). Its fast signal is used for the first level trigger and together with the signal from the Scintillat-

ing Electromagnetic Calorimeter (SE) it can be used for particle identification with the ΔE-E method.

The SCS comes next, it provides the magnetic field necessary for use of the MDC. It is very thin to avoid energy loss and particle showers. The SE is placed at the most outer side, as a calorimeter inside a magnetic field would require the use of less precise photodiodes instead of photomultipliers.

2.3.2.1. Mini Drift Chamber (MDC)

The Mini Drift Chamber consists of 1738 drift tubes in 17 different cylindrical layers and covers scattering angles from 24^0 to 159^0 (Fig. 2.6 and Fig. 2.7). The tubes are made of Mylar foil coated with aluminium on the inside. In the center there is a sensing wire made of gold plated tungsten. The MDC can measure polar and azimuth angle and momentum of charged particles. A detailed description can be found in Ref. [18].

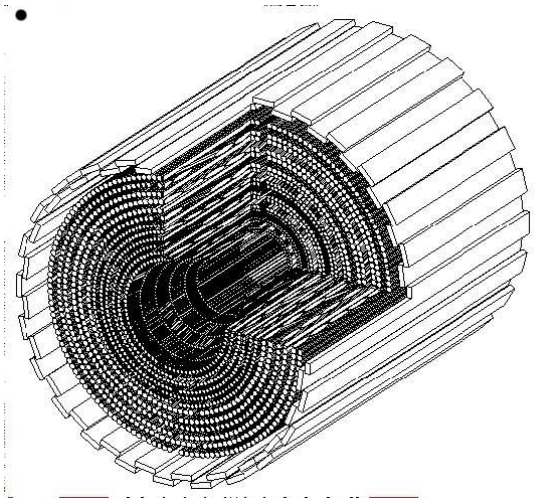

Figure 2.6.: CAD view of Mini Drift Chamber (MDC) from Ref. [17]

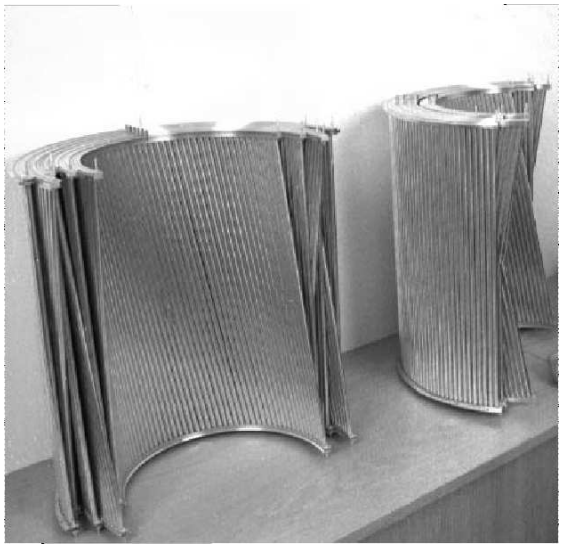

Figure 2.7.: Drift tubes from Ref. [17]

2.3.2.2. Plastic Scintillator Barrel (PS)

The Plastic Scintillator Barrel is a cylindrical detector made up of 3 parts: forward (PSF), central (PSC) and backward (PSB), see Fig. 2.8. All are made up of 8 mm thick straight bars of plastic scintillators. PSF and PSB are caps at both ends of the barrel and consist of 48 cake-piece shaped elements. PSC is cylindrical around the beam axis and consists of 50 elements, since 2 holes had to be made for pellet target tubes. Read out is except for these 2 elements at both ends, allowing to determine position. The main purpose of PS is for fast triggering in the Central Detector, but in conjunction with SE or MDC the deposited energy can be used for particle identification with the ΔE-E and ΔE-P methods. It also provides timing information for MDC.

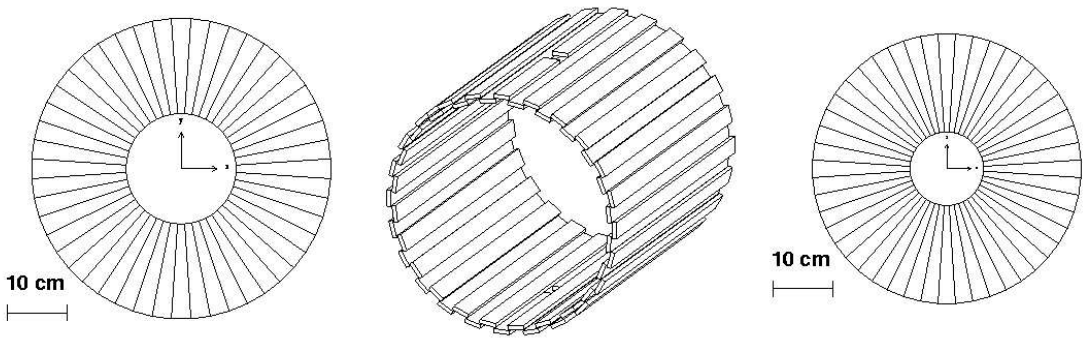

Figure 2.8.: Plastic Scintillator Barrel, forward (PSF), central (PSC) and backward (PSB) parts from Ref. [17]

2.3.2.3. Superconducting Solenoid (SCS)

The SCS provides the axial magnetic field necessary for the MDC to measure particle momentum. A field strength up to 1.3 T is possible, although 1 T is the most often used strength. As it is inside the calorimeter, it was designed extra thin to avoid energy losses of passing particles. An iron yoke confines the magnetic field and thereby protects the photomultipliers in calorimeter and the readout electronic.

Coil	
Inner/outer radius (mm)	276.8/288.8
Total winding length (mm)	465
Conductor (stabilizer)	NbTi/Cu (pure Al)
Cooling	Liquid He, conduction
Maximum central magnetic flux density, Bc (T)	1.3
Field uniformity in the MDC (T)	1.220.25
Cryostat	
Material	Aluminium
Inner/outer radius (mm)	245/325
Overall length (mm)	555
SCS wall thickness (coil+cryostat) (radl)	0.18

Table 2.2.: Properties of Superconducting Solenoid

2.3.2.4. Scintillating Electromagnetic Calorimeter (SE)

The outermost part of the Central Detector is the Scintillating Electromagnetic Calorimeter (Fig. 2.9). It consist of 1012 sodium doped caesium iodide scintillating crystals and covers a angular range from 20° to 169°. The crystals have the form of a truncated pyramid and are arranged in 24 layers along the beam axis. In the forward part the layers have 36 elements (gray), in central

part 48 (white) and in backward part 24 and 12 (black). The main purpose of the SE is the energy measurement of neutral tracks, since the energy of charged can also be derived from the MDC. Some of the design parameters of the SE are listed in Table 2.3.

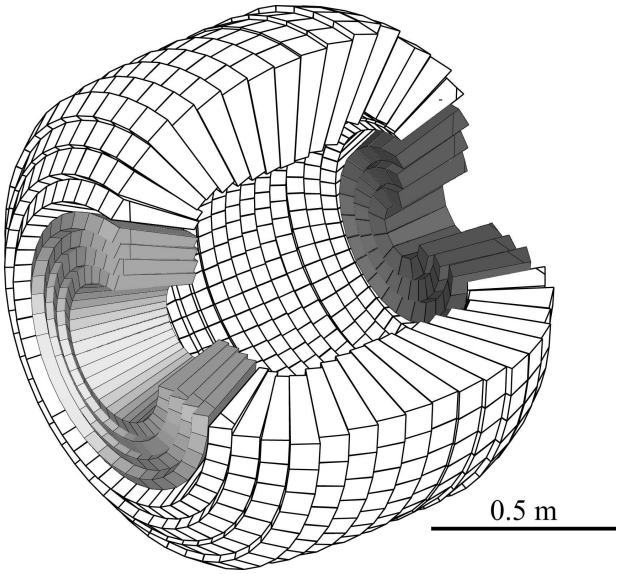

Figure 2.9.: Scintillating Electromagnetic Calorimeter (SE), beam direction to the right from Ref. [17]

2.3.3. Forward Detector (FD)

The Forward Detector covers an angle of 3° to 17° and is designed to measure charged particles precisely. The Forward Detector has 9 layers with different types of plastic scintillators and 1 layer with drift tubes. These many layers allow to identify charged particles by ΔE-E technique.

ΔE-E technique is best, when the particles are stopped, which is the case for protons with energies up to 0.3 GeV, deuterons up to 0.4 GeV and charged pions up to 0.17 GeV. Some of the design parameters of the Forward Detector are listed in table 2.4.

2.3.3.1. Forward Window Counter (FWC)

Downstream the first detector of the Forward Detector is the Forward Window Counter (Fig. 2.10), which consist of 12 plastic scintillator elements with a thickness of 5 mm. Its purpose is to reduce the background from beam/beampipe interaction. To fit well to the scattering chamber its elements have been inclined by 19° from vertical position. Since it is small and fast it is often used as first level trigger.

SE design parameters	
Amount of sensitive material (g/cm2)	135
radiation length	≈16
nuclear interaction length	≈0.8
Geometric acceptance	96%
Polar angle (degree)	≈20-169
Azimuth angle (degree)	≈0-360
Max kinetic energy for stopping	
μ/proton/deuteron	190/400/500
Scattering angle resolution (degree)	≈5 (FWHM)
Time resolution (ns)	
Charged particles	5 (FWHM)
Photons	≈40 (FWHM)
Energy resolution	
Charged particles	≈3% (FWHM)
Photons	$\approx 5\%/\sqrt{E(GeV)}$ (RMS)

Table 2.3.: SE design parameters

Total number of scintillator elements	280
Scattering angle coverage (degree)	3-17
Scattering angle resolution (degree)	0.2
Amount of sensitive material (g/cm2)	50
Radiation length	≈1
Nuclear interaction length	≈0.6
Thickness of vacuum window (st. steel) (mm)	≈0.4
Maximum kinetic energy (Tstop) for stopping:	
μ/proton/deuteron/alpha (MeV)	170/300/400/900
Time resolution (ns)	<3
Energy resolution for	
Stopped particles	≈ 3%
Particles with Tstop < T< 2Tstop	4∼8%
Particle identification	ΔE-E

Table 2.4.: Forward Detector design parameters

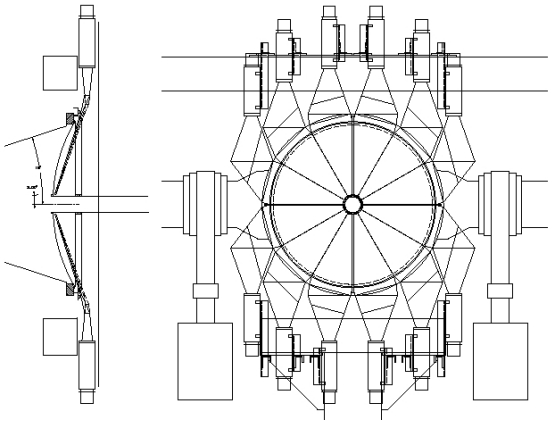

Figure 2.10.: Forward Window Counter (FWC) from Ref. [17]

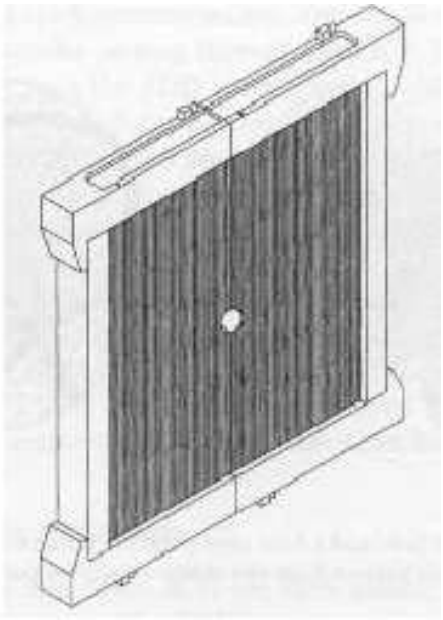

Figure 2.11.: Forward Proportional Chamber (FPC) from Ref. [17]

2.3.3.2. Forward Proportional Chamber (FPC)

The Forward Proportional Chamber (Fig. 2.11) is next in the Forward Detector. It was planned to be made of 4 modules, but when the data analysed in this work was taken, only 2 modules were mounted. They were rotated towards each other by 90^0. Each module consist of 4 layers with 122 drift tubes. The thickness of the drift tubes is 8 mm. This allows a very precise tracking of charged tracks.

2.3.3.3. Forward Trigger Hodoscope (FHD)

The Forward Trigger Hodoscope, also called Juelich Hodoscope (Fig. 2.12), is made of 3 layers of 5mm thick plastic scintillators. The first two layers in beam direction have each 24 Archimedian spiral shaped elements, whereas the third has 48 cake piece shaped elements. This allows a special pixel structure, which helps resolving multi-hit-ambiguities.

2.3.3.4. Forward Range Hodoscope (FRH)

The Forward Range Hodoscope (Fig. 2.13) is made of 4 layers each with 24 plastic scintillator elements. The thickness of each layer is 110 mm. Due to the large thickness of the layers much energy is deposited by charged particles, therefore the FRH allows precise energy reconstruction. Particle ID reconstruction is also possible because, together with the FHD, the many layered

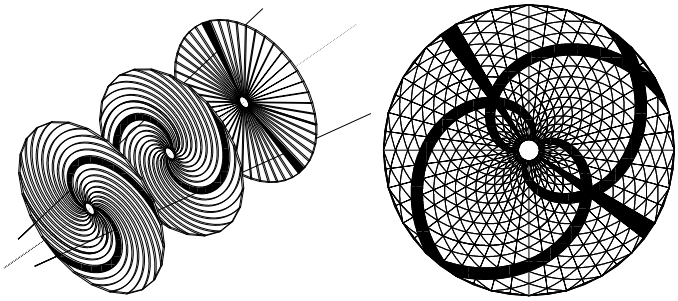

Figure 2.12.: Forward Trigger Hodoscope (FHD) from Ref. [17]

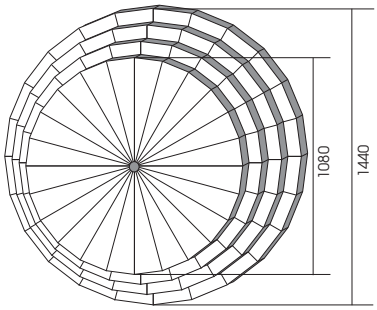

Figure 2.13.: Forward Range Hodoscope (FRH) from Ref. [17]

design allows for many different ΔE-E plots. It is also possible to reconstruct energy of particles that interacted hadronically.

2.3.3.5. Forward Range Intermediate Hodoscope (FRI)

The Forward Range Intermediate Hodoscope (Fig. 2.14) is positioned between the third and fourth layer of the FRH. It consists of 32 vertical and 32 horizontal 5mm thick plastic scintillator bars. The bars have a width of 30 mm close to the beampipe and 60 mm farther away from beampipe. FRI was designed to measure the angle of neutrons by detecting the recoil proton from hadronic interaction. The probability of detecting a neutron with FRI is about 35%.

2.3.3.6. Forward Veto Hodoscope (FVH)

As the last detector of the Forward Detector the main purpose of the Forward Veto Hodoscope (Fig. 2.15) is to identify punch-through tracks. Its signal is also used for some trigger conditions. It is made of 12 bars of plastic scintillator 137 mm high, 1650 mm long and 20 mm thick. The bars have photomultipliers at both ends. This allows to determine hit position by timing difference.

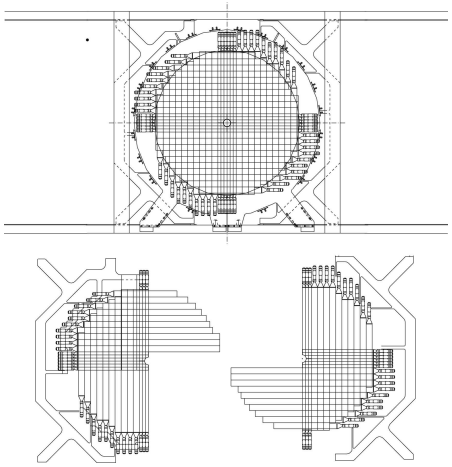

Figure 2.14.: Forward Range Intermediate Hodoscope (FRI) from Ref. [17]

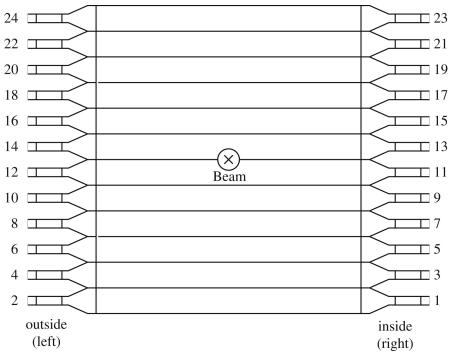

Figure 2.15.: Forward Veto Hodoscope (FVH) from Ref. [17]

2.3.4. Data acquisition system (DAQ) and triggers

All detectors together have about 1500 charge to digital converter (QDC) and 4000 time to digital (TDC) converter channels. With pedestal suppression the average size of the data for a single event is 2-3 kB. With a luminosity of $10^{32} cm^{-2} s^{-1}$ elastic pp reactions alone would have an event rate of several million per second, which is far beyond the capabilities of the readout system and would produce a lot of uninteresting events. Therefore a complex trigger system has to determine which are desired events and which can be ignored. The data acquisition system is sketched in Fig. 2.16.

The most important aspect is, that the signals are all split into two branches. One branch is delayed by 300 ns, leaving enough time for the other branch to pass through the trigger system and generate stop or readout signals.

The trigger system has two levels. The first uses signals from the fast plastic scintillators to trigger the hardware acquisition. The second level uses the signals from the slow electromagnetic calorimeter and generates a fast-clear signal if second level trigger conditions are not met. This prevents the start of the readout.

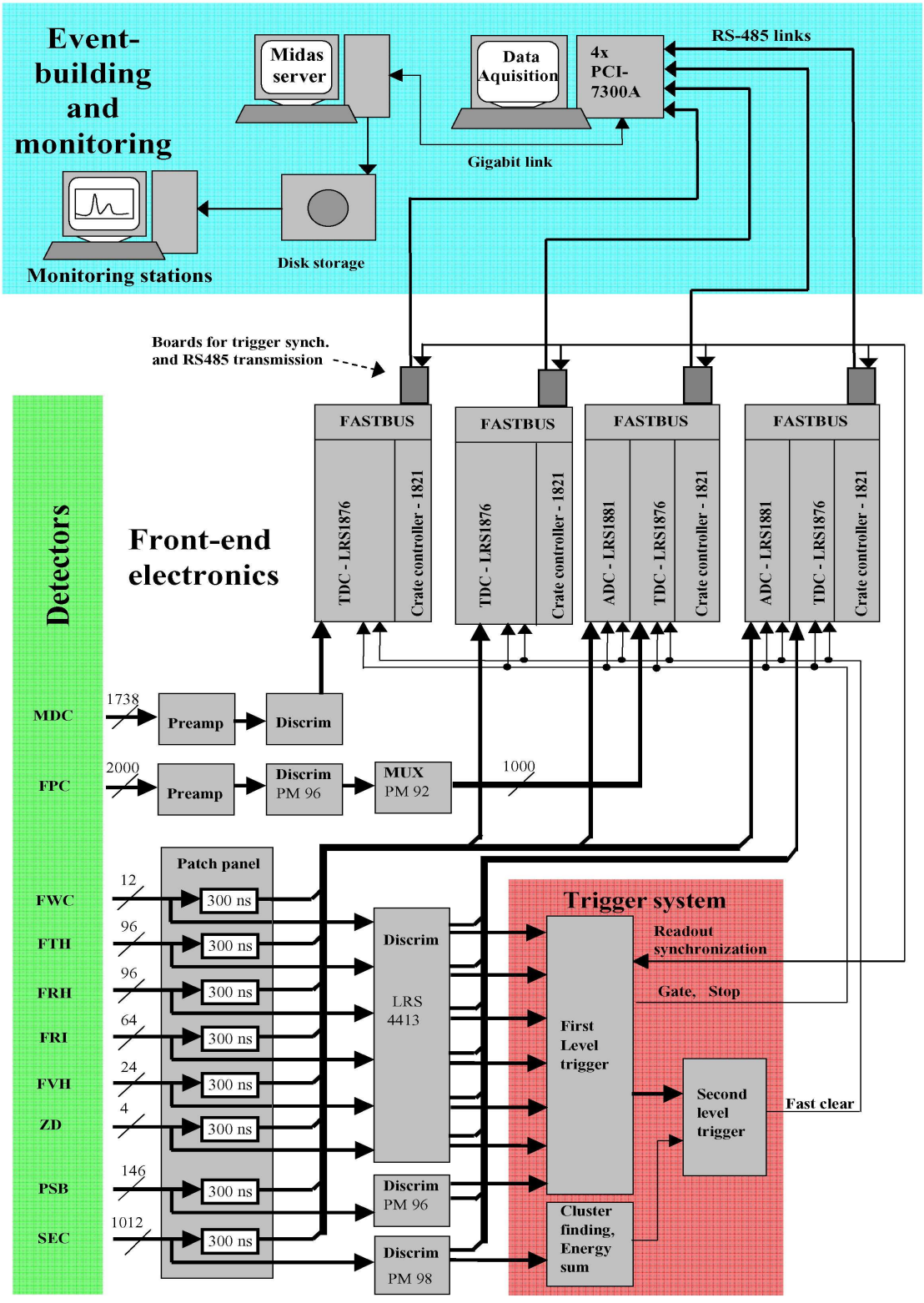

Figure 2.16.: Structure of the DAQ and trigger system from Ref. [17]

3. Analysis software and methods

The output generated by the detector and the subsequent data acquisition system deliver the identification number of the fired detector components, timing (TDC) and signal height (QDC) information. Translating this raw information into physically relevant information like directions, velocities and energies is the task of the analysis software. This is done by the W4P event reconstruction program, which identifies tracks and the deposited energy related to the track.
With this track information one has to identify the events with the desired particles using cuts and an artificial neural network (neural net). The angles and energy of a track can still be slightly off due to limited detector resolution, but this can be improved by applying energy and momentum conservation in a kinematical fit.
These results still have little physical meaning, since they are convolved with the acceptance and efficiency of the WASA detector. Hence an efficiency and acceptance correction is required. This is done by simulating events of the reaction-type in question using either pure phase space or a distinct model and measuring these reactions with a virtual detector and analysing them the same way as real data. By dividing these spectra by the spectra of the purely generated events, the efficiency and acceptance can be determined. The flow chart of the analysis is shown in Fig. 3.1.

3.1. Event generation

The basis for the event generator GIN is the FOWL program, which is part of the CERN program library. Within kinematical constraints it generates random momentum vectors of all particles. The events are created with phase space weights and a model can be applied by multiplying the appropriate amplitudes. For the further analysis the weights are removed. Their effect upon the spectra are preserved by generating a random number for each event between zero and maximum weight and dropping those events, which have a weight smaller than the random number. With this procedure events with a high weight are more likely to remain, therefore the shape of the spectra does not change.

3.2. Monte Carlo simulation

The Monte Carlo simulation WMC uses the GEANT3 software package from CERN. By having the entire detector volume defined in GEANT terms, the interaction of every particle with the detector and dead material and the following detector output can be simulated. The input are the momenta of the particles as they are generated with GIN. From the user defined vertex position the movement of the particles through the detector is simulated on a step-by-step basis. In each step the probability of interaction, decay or scattering is calculated for each track according to

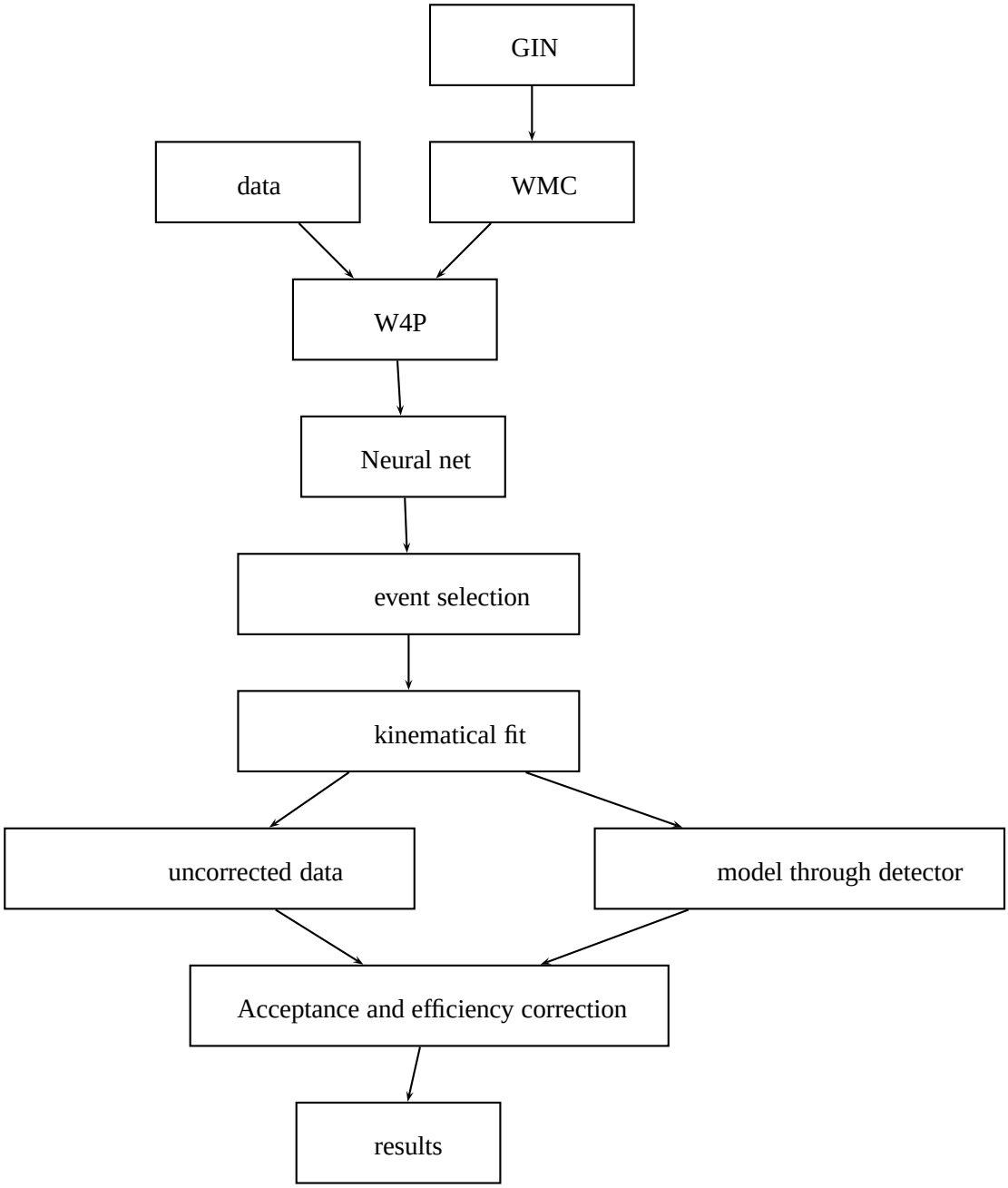

Figure 3.1.: flowchart of analysis

known physics and each effect is randomly chosen with its calculated probability. All primary and secondary tracks are followed this way till all are outside the detector volume. The output format is nearly identical to the format of the data, which allows to use the same methods for analyzing as used for real data. Detector changes from run to run are accounted for by using the alignment files, which contain the detector description in GEANT language.

3.3. W4P Event reconstruction

The track and event reconstruction was done using W4P, the standard program with WASA for reconstruction. Starting with this program Monte Carlo simulations and data are treated the same way. W4P processes all the steps necessary for identifying tracks in the detector, like conversion of QDC into deposited energy, conversion of TDC information into time clustering of hits, track finding. With W4P it is also possible to do particle identification and cuts.
Since a neural net written in C++ was used for particle identification and W4P is in Fortran, W4P was only used for track reconstruction and the tracks were stored in N-tuple format and neural net and cuts were applied later.

3.4. ΔE-E technique

Normally particle identification in the Forward Detector in case of charged particles is done by the ΔE-E technique. Since the energy deposited in the different detector layers all depend on the particle and the energy of the particle, different particles create in a scatter plot of deposited energy of one detector layer versus energy or deposited energy of another layer a signal in particle specific areas called bands. An example is shown in Fig. 3.2, where a deposited energy is plotted versus the full energy. Many other different scatter plots for identification are possible, each deposited energy of one of the ten Forward Detector layers versus the deposited energy of another layer is a scatter plot in which different bands are visible. Most useful for this work are deposited energy in one Forward Range Hodoscope layer versus deposited energy in another Forward Range Hodoscope layer, as these layers are the thickest.

The position of these bands is dependent on charge and mass of the particle. Therefore particles can be identified by the position in a ΔE-E scatter plot. Fig. 3.2 does not show the entire bands. The possible energy, that the specific particles can have due to reaction kinematics and beam energy determine, which part of the band shows up. The part of the band correlated with higher energies, bend at a certain point back towards the origin of the plot. The reason is, that at high enough energies the particles are not stopped inside the detector and an increase in kinetic energy does no longer increase, but decreases the deposited energies. In case of even higher energies the particles become minimum ionizing, which causes the high energy end of all bands to be near the origin of the plot, since minimum ionizing particles deposit nearly the same energy in all detector layers independent of particle type. In this case the bands are too close to each other to be separable. Therefore with increasing energy the ΔE-E technique is less and less effective in identifying particles, identification being impossible in the case of very high energies.
In the case of this analysis the particles are not yet minimum ionizing, but already have such a

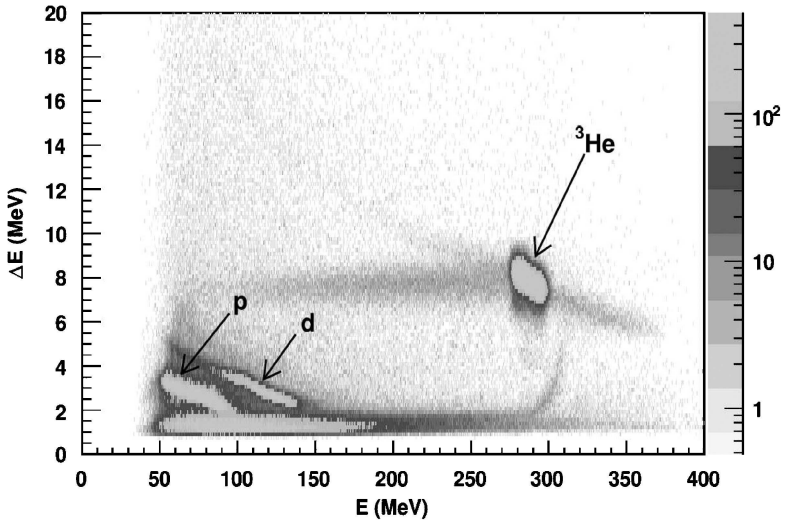

Figure 3.2.: Example of ΔE-E event distribution from Ref. [17]

high energy, that a large part of the deuteron band overlaps with the proton band. The reaction $pp \rightarrow pp\pi^0$ has a far higher cross section than $pp \rightarrow d\pi^+\pi^0$, but the same number of neutral and charged tracks, therefore it constitutes the largest background reaction for this analysis. A neural net had to be used for an improved ΔE-E analysis.
In case of $pp \rightarrow pn\pi^+\pi^0$ the neutron was not measured, therefore $pp \rightarrow pp\pi^0$ has a similar role as the main background and the neural net was also used.

3.5. Neural Net

The position of a particle inside the band is dependent on the energy. The deuterons that overlap are the high energy deuterons, whereas the protons that overlap with them are not the highest energy protons. This implies, that when applying the correct cuts to all possible ΔE-E plots, deuteron and protons can be distinguishable to some extent even if a single ΔE-E plot is not sufficient. Evaluating all these plots by hand is impractical, especially since one cannot look at the plot containing all information - the 10 dimensional plot of all deposited energies versus all other deposited energies.
What is needed is an algorithm that maps the 10 deposited energies to whether it is a proton or deuteron. The best solution for such a problem is a neural net trained on particle identification based on all deposited energies. The neural net used was developed by M.Bashkanov, a description can be found in Ref. [19]

3.6. Particle identification in Central Detector

The main method to identify charged particles in the Central Detector is the ΔE-P technique using the momentum information from MDC. Neutral tracks do not have a curvature, as they are

constants	FRH1	FRH2	FRH3	FRH4	punch through
C_0	2.03227	0.468512	0.768832	9.1301	11.8193
$C_1[GeV^{-1}]$	-67.2193	-15.9898	-14.5199	-45.4404	-78.5049
C_2	0.219912	-1.58284	-1.9609	-0.716251	3.58860
$C_3[GeV^{-1}]$	-9.19007	-0.549665	0.206675	-2.93309	-15.445
C_4A5	1.37639	27.1494	30.597	7.11065	1.96028
$C_5[GeV^{-1}]$	-120.31	-214.319	-156.116	-36.207	-12.2744
C_6	-0.925965	-1.42227	-2.63549	-17.2432	-0.0852235
$C_7[GeV^{-1}]$	-18.5342	-12.9962	-7.04743	37.461	0.280786

Table 3.1.: Coefficients for energy reconstruction

unaffected by the magnetic field, and the cluster size and energy deposition allows to distinguish neutrons and photons. Particles, that decay inside the Central Detector, can be identified by the invariant mass of the decay particles.

3.7. Energy reconstruction

The relation of deposited energy to real kinetic energy for deuterons can be approximated by 5 formulae, one formula each for deuterons stopped in FRH1, FRH2, FRH3, FRH4 and punch-through, respectively. The general structure for all formulae is the same:

$$E_{kin} = [1 + e^{C_0+C_1E_{dep}} + e^{C_2+C_3E_{dep}} + e^{C_4+C_5E_{dep}} \cdot \theta + e^{C_6+C_7E_{dep}}] \cdot E_{dep}$$

E_{kin} is the kinetic energy of the particle , E_{dep} the deposited energy and θ the scattering angle of the particle, which is the angle between the momentum vector and the beam axis.
The coefficients were determined by passing simulated $pp \rightarrow d\pi^+$ events through the virtual detector and selecting the tracks stopped in the respective detector or punch through tracks. For these tracks the true deuteron energy was known and a fit of the formula to the E_{dep} versus E_{kin} scattering plot yielded the coefficients shown in table 3.1.

3.8. Kinematical fit

Due to the limited detector precision a kinematical fit was applied to improve the data.
Input for the kinematical fit are the measured energies and angles along with their errors. Energy and momentum conservation are used to calculate the unmeasured pion energy.
The kinematical fit applies small changes - calculated using Lagrangian multipliers - until energy and momentum conservation are fulfilled or the maximum number of steps is exceeded. As measure for the quality of the fit, χ^2 is calculated.
In the ideal case the χ^2 distribution of all events vanishes at zero and peaks at the number of degrees of freedom. In reality this depends on whether the selected errors are equal to true

errors and whether the reduced χ^2/deg. of freedom (peak around 1) or just χ^2 (peak at number of degrees of freedom) is plotted.

4. Event selection

4.1. Trigger selection

As only a limited rate of events can be written on tape, a first selection happened already during data taking in form of the trigger. Therefore choosing the right trigger was very crucial. In the case of this analysis the task was even more difficult, since the triggers for the run were not tailored towards $d\pi^+\pi^0$ or $pn\pi^+\pi^0$ but towards other reactions. For a list of the triggers see Appendix A.1.

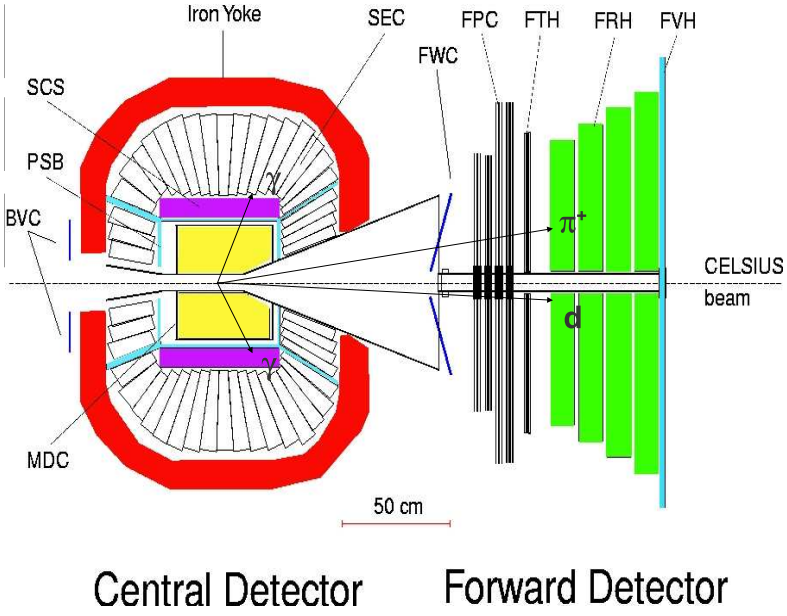

Figure 4.1.: WASA detector from Ref. [17]

The reaction $pp \rightarrow d\pi^+\pi^0$ was analysed using data taken at T_p=1.1 GeV. Due to kinematical restrictions deuterons have $\theta < 16^\circ$ and go therefore only into the Forward Detector. θ is the scattering angle, the angle between momentum vector of particle and beam axis. The π^0 decays almost instantly, before reaching any detector into two γs, which can go in any direction. But the Forward Detector is not suitable for detecting γs. The θ angle of the π^+can be up to 160°, though most π^+ have $\theta < 50^\circ$.

Since having both π^+ and deuteron in the Forward Detector makes particle identification in the Forward Detector more difficult, it is more sensible to choose a trigger, which allows the π^+ only in the Central Detector. The trigger should require one charged track in the Forward Detector, one charged and two neutral tracks in the Central Detector.

Most triggers are not suited, since they either require no hit or two hits in the Plastic Scintillator Barrel. Events, where in reality one charged track is in the Central Detector, cannot satisfy this condition if they are well measured. So only events with missed hits or garbage could be selected with such triggers. Other triggers are not suitable, because they have very limited requirements and therefore allow a lot of other reactions, e.g. $psc1 * frha1$ requires one hit in the central part of the Plastic Scintillator Barrel, one hit in the first range of the Forward Window Counter and has no other restrictions. This allows for $d\pi^+\pi^0$, but also for practically anything else, especially elastic pp. Such reactions with high cross section require the trigger to have a high prescaling factor. When only every thousandth event or even less is written, no useful amount of data for $d\pi^+\pi^0$ is available from the trigger.

The most promising triggers are $secc f1 * Pwc1hdsrh1ps1$ and $secc f2 * Pwc1hdsrh1ps1$. The part $Pwc1hdsrh1ps1$ is a pretrigger which requires one hit in the Plastic Scintillator Barrel and one hit in the Forward Window Counter, one hit in the Juelich Hodoscope and one hit in the Forward Range Hodoscope, which fits one π^+ in the Central Detector and one deuteron in the Forward Detector quite well.

$secc f1$ requires two clusters in the calorimeter. Clusters are any group of hits in neighboring elements, so a γ passing through two neighboring elements of SE will be counted only as one cluster. $Secc f2$ is the same, just three clusters. As the π^+ is likely to create a hit in SE and the γs do also create hits in SE, this trigger would fit the requirements of one or two neutral and one charged track in the Central Detector and one charged track in the Forward Detector.

Unfortunately the trigger did not work properly. Independent of cuts, application of kinematical fit, detector calibration, use of neural net or used model for acceptance correction the results show a strongly asymmetric d and π^0 center of mass θ angle distribution:

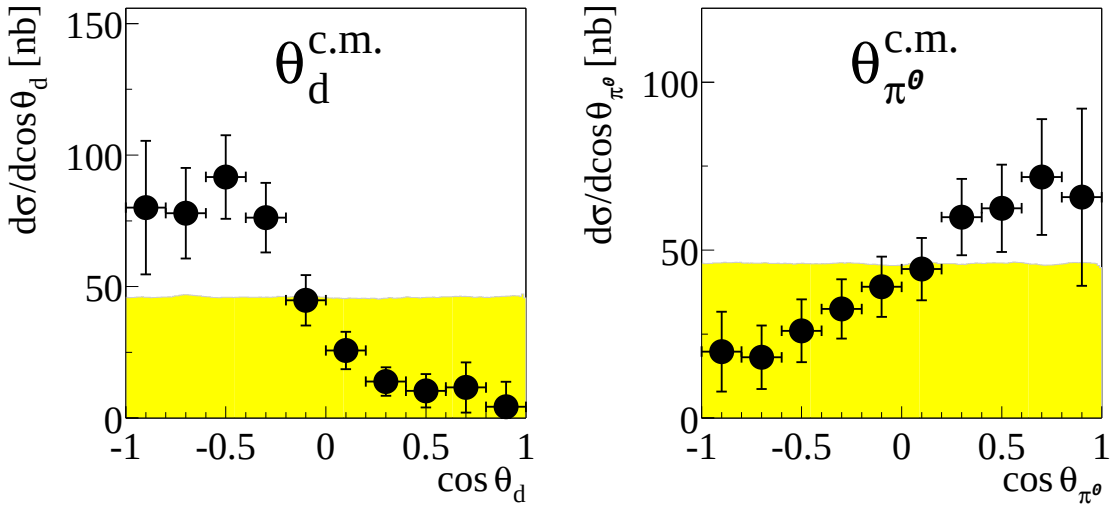

Figure 4.2.: θ_d^{cm} and $\theta_{\pi^0}^{cm}$ in case of π^+ in CD

Fig. 4.2 shows these plots and the asymmetry is beyond statistical errors. Since the entrance channel is symmetric, the exit channel has also to be symmetric in the center of mass system.

This shows, that there is a serious error in this data set. A first thought could be, that there is still a large background, e.g. ppπ^0, which could produce such effects, since for calculation of center of mass angles the mass is used and with misidentified particles the wrong masses are used. This could cause an asymmetry.

But selecting the reaction $pp \rightarrow pp\pi^0$ with the same trigger gives for the center of mass angle of π^0 the same asymmetrical distribution. Therefore miss identification is unlikely to be the cause of the asymmetry.

The cause unfortunately is in the end, the triggers, which at a first look seemed to be very good for the reaction. This can be shown by comparing both triggers, which differ only due to $seccf1$ and $seccf2$. As anyway three tracks, one charged and two neutral, are selected in the Central Detector, the difference between a trigger requiring two cluster and one requiring three clusters should be very small, as three tracks in the Central Detector will likely produce three clusters most of the time. The only exception is, when two tracks pass the SE close to each other and the fired detectors are so close, that they are counted as one cluster.

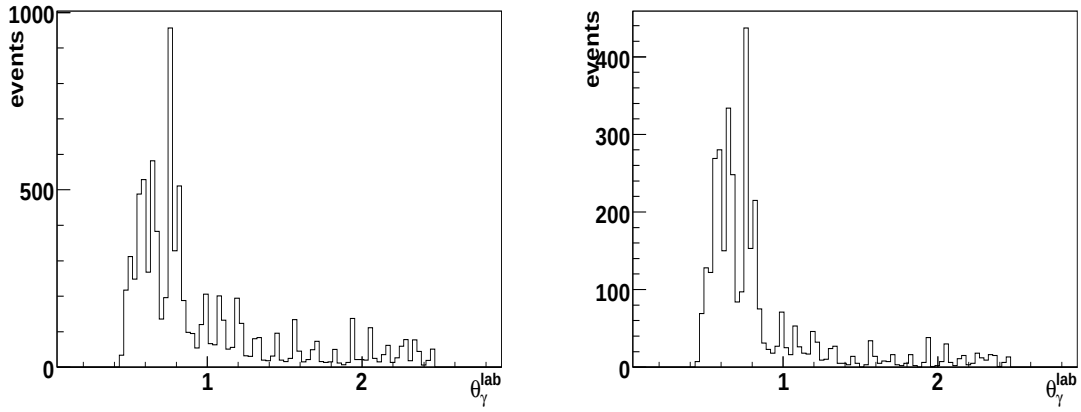

Figure 4.3.: θ_γ^{lab} with 2 cluster (left) and 3 cluster (right) trigger

Figure 4.3 shows the θ angle of both γs in the lab system after selection of d$\pi^+\pi^0$ using the seccf1 trigger. The 2 γs from π^0 decay and the π^+ normally produce not only two but three clusters in SE. Therefore the figures should look nearly the same, as their only difference is the requirement of two or three clusters. But Fig. 4.3, right side, shows a reduction of events by about 60% with more events lost outside the region between 0.45 rad and 0.85 rad than inside this region.

Whereas the requirement of three clusters instead of two should reduce the amount of events, it should be only a few percent effect. But more importantly the effect should not have such a strong angular dependence. Between 0.45 and 0.85 rad the loss is 50-55% whereas outside the loss is more around 75%.

The only change between both figures is the used trigger. Since the trigger should not have such an effect, the explanation is, that the trigger had some kind of undocumented malfunction.

The most plausible explanation for the nature of this malfunction is, that the trigger did not react to all clusters in SE, but only to the clusters in the angular region roughly between 0.45 and

0.85 rad. First, this is plausible, because for cluster detection the connection of different elements to the trigger were done layer-wise, so that an entire layer was either connected or disconnected. A malfunction there would cause the trigger to miss clusters at certain angles, whereas detecting clusters at other angles. And the second assumption, that clusters, that actually fired the trigger, have to be between 0.45 and 0.85 rad, explains both pictures. In Fig. 4.3 left side the area between 0.45 and 0.85 rad is pronounced, but there are still a lot of events elsewhere. This is to be expected, since only two clusters have to lie inside the region. In cases where one is provided by the π^+ the second γ does not have to hit in the region. Therefore the greater part of events should be in this region, but outside should be still some events.

When requiring three clusters inside this angular region, the γs should be far more concentrated there, because only when there is some garbage cluster the trigger could fire with one γ outside this region. A similar angular distortion happens for the π^+. As this distortion is not simulated in the model, the acceptance corrected data has to be asymmetric.

Since this problem reduces the number of events very much and is very hard to simulate - the trigger could still sometimes react to clusters outside the region -, only solution is to use a different trigger.

There are no other promising triggers which allow π^+ in the Central Detector, so a trigger with a π^+ in the Forward Detector has to be used.

A suitable trigger is $ecf2 * Vpsd * Pfhdw2Vps$. $Pfhdw2Vps$ is a veto on lastic Scintillator Barrel hits and the requirement to have two matching clusters in the Juelich Hodoscope and the Forward Window Counter. Both requirements fit two charged forward tracks and no charged central track. $Vpsd$ is a further delayed Veto on the Plastic Scintillator Barrel. $ecf2$ requires signals in the forward and central part of SE, which indicate energy deposition above a certain rather low threshold. As this could lead to some slight limitation in π^0 angle, observation of a symmetric π^0 distribution will be important to rule out this possibility.

Keeping this possible limitation in mind, the trigger is suitable for the reaction. The basic requirement apart from the trigger is two neutral tracks in the Central Detector - γ from π^0 decay - and two charged tracks in the Forward Detector - deuteron and π^+.

For the channel $pp \rightarrow pn\pi^+\pi^0$ the same trigger had to be used. Although both the proton and the pion can have high angles and therefore could be detected with the Central Detector, all triggers allowing 2 or more hits in the Plastic Scintillator Barrel require 1 or more hit in some Forward Detector layers. As the neutron has only a chance of about 35% to interact with any layer, the chance to interact with a specific layer is too low to have enough events from such triggers.

In summary on can say, that the triggers were not tailored towards $pp \rightarrow d\pi^+\pi^0$ and $pp \rightarrow pn\pi^+\pi^0$. Those, which allowed one charged track in the Central Detector and seemed suitable, had a malfunction causing a asymmetric angle distribution in center of mass system. Therefore a trigger had to be used, which allowed no charged tracks in the Central Detector. So π^+ and d or p were both measured and had to be identified in the Forward Detector.

4.2. Reaction $pp \rightarrow d\pi^+\pi^0$

4.2.1. π^0 identification

Since the trigger allows only neutral tracks in the Central Detector and since the number of tracks has to be two, the tracks in the Central Detector can only be γs from π^0 decay, freely produced γs, neutron or background. All the possibilities except the π^0 decay are unlikely to happen. Therefore the invariant mass of the two γs should show a very distinct peak at the π^0 mass.

Figure 4.4 shows the invariant mass spectra of the two neutral tracks in the Central Detector for data and model in the region around the π^0 mass, without any further restrictions like energy or number of forward tracks. The visible background in the data is from single γ production, where some background was mistakenly identified as second neutral track. It is very small around the π^0 mass, therefore a rather broad cut with $0.09 < M_{\pi^0} < 0.2$ selects nearly all π^0 with little background.

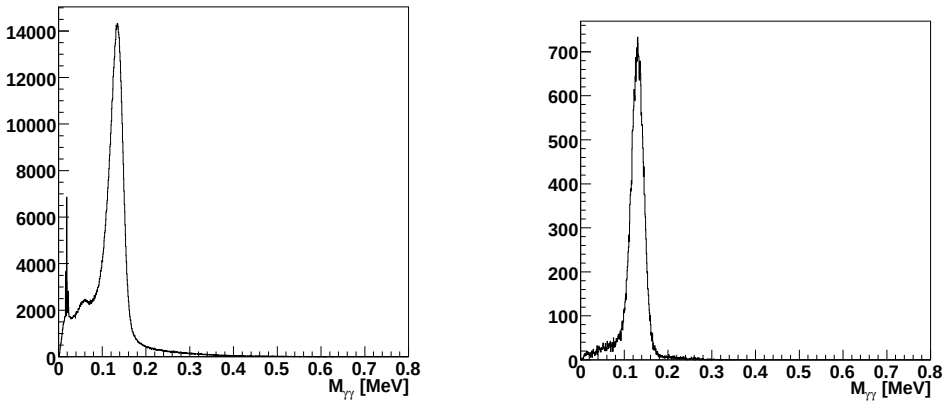

Figure 4.4.: $M_{\gamma\gamma}$, left for data, right for simulation

4.2.2. Deuteron and π^+identification

A few simple cuts are used - nearly all deuterons are kinematically limited to $\theta < 15^\circ$ and cannot stop before the 3rd layer of range hodoscope - but mainly for deuteron and π^+ identification the neural net described in section 3.5 is used.

The normal procedure would be to identify charged particles by ΔE-E technique. Fig. 4.5 shows a ΔE-E plot for a beam energy of 1.1 GeV. There is a large overlap between deuterons and protons, in data the deuterons are nearly not visible. Since so far only a cut for π^0 is done, all pp$\rightarrow$ppπ^0 events are still present. With a cross section larger by a factor of 50 this background threatens to prevent any meaningful results for d$\pi^+\pi^0$.

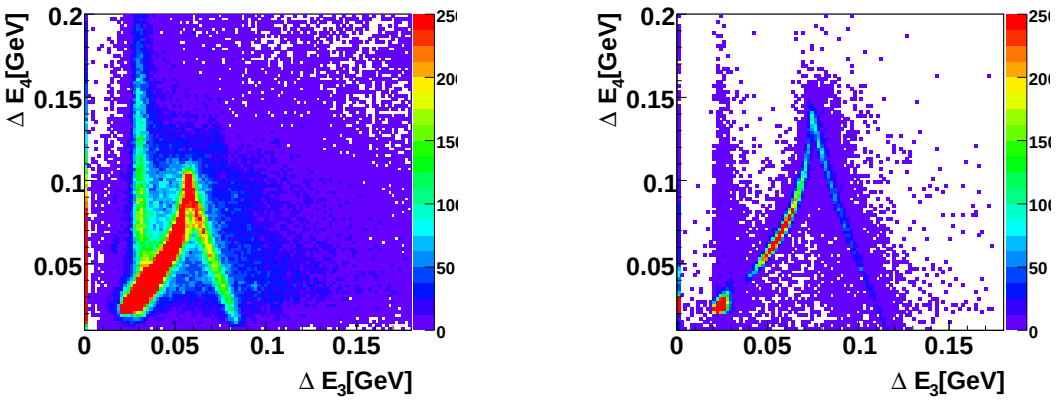

Figure 4.5.: Deposited energy in 4th Forward Range Hodoscope versus deposited energy in 3rd Forward Range Hodoscope, left data, right simulation $pp \rightarrow d\pi^+\pi^0$

Only the stopped deuterons can be separated from the protons. As about 50% of the deuterons are punch-through, this would reduce statistics significantly. But due to the high cross section, some ppπ^0 could remain. Trying some ΔE-E cuts without losing the punch-throughs gives unsatisfactory results shown in Fig. 4.6, some remaining protons are clearly visible, even simulated protons are not sufficiently removed.

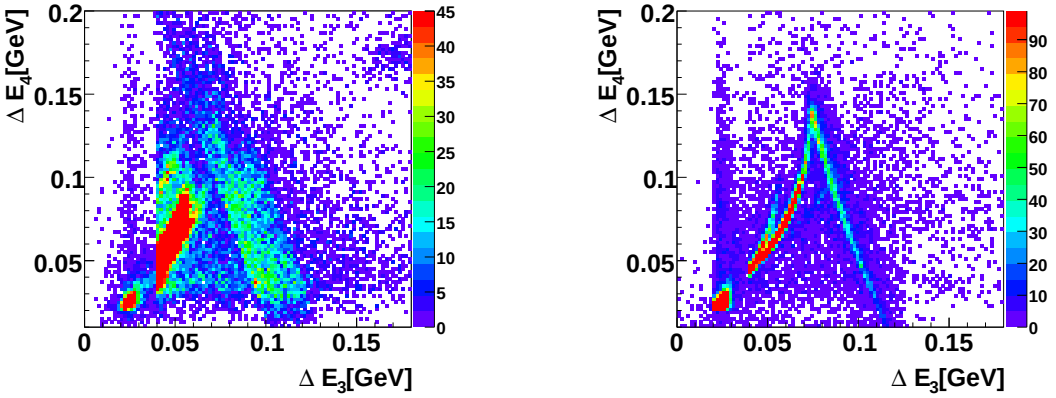

Figure 4.6.: Deposited energy in 4th Forward Range Hodoscope versus deposited energy in 3rd Forward Range Hodoscope, left data, right simulation containing both $pp \rightarrow d\pi^+\pi^0$ and $pp \rightarrow pp\pi^0$, several cuts applied

This problem can be lessened by looking at several different ΔE-E plots and cuts both for deuterons and pions. The pions appear mostly in the bottom left corner on such plots. For two protons to be misidentified in this selection as a pion and a deuteron can only happen if both protons are punch-through and one is in the pion region of several plots and the other in the deuteron region of several plots.

But the problem is solved best by taking all energy information in the Forward Detector and looking at the plot containing all information - the 10 dimensional plot $\Delta E_1 vs \Delta E_2 vs ... vs \Delta E_{10}$. Whereas this cannot be done by the human eye, numerically a neural net trained by the 10 energy inputs of simulated particles is able to do that.

The result is shown in Fig. 4.7. In the data there is no longer a proton band visible and the deuteron band is very similar to the one of the simulation, only few background events remain.

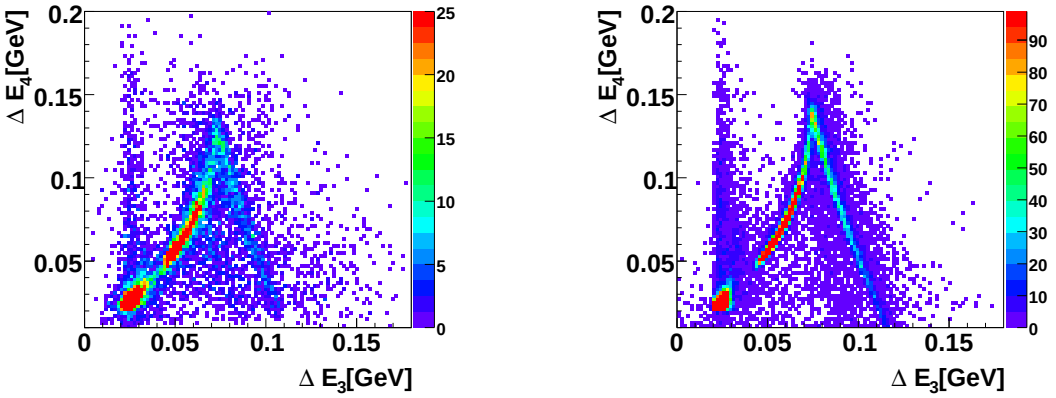

Figure 4.7.: Deposited energy in 4th Forward Range Hodoscope versus deposited energy in 3rd Forward Range Hodoscope, left data, right simulation containing both $pp \rightarrow d\pi^+\pi^0$ and of $pp \rightarrow pp\pi^0$, neural net applied

To estimate the remaining background of $pp\pi^0$ events the numbers of the remaining simulated $d\pi^+\pi^0$ and $pp\pi^+$ events after different cuts can be compared (Table 4.1).

Reaction	Before	Cuts ΔE-E	Stopped	Neural net
$d\pi^+\pi^0$	566545(100%)	21727(3.8%)	10564(1.8%)	21241(3.7%)
$pp\pi^+$	1297191(100%)	5541(0.4%)	339(0.02%)	57(0.004%)

Table 4.1.: Remaining simulated events

The low acceptance is mainly due to the condition of π^+ hitting the Forward Detector, since it can have θ angles up to 150°, whereas the Forward Detector covers only θ up to 17°.

The ΔE-E cuts alone are insufficient, as $pp\pi^0$ has a 50 times higher cross section than $d\pi^+\pi^0$, which would mean about 5 times more protons than deuterons. This is consistent with the results from data, where in figure 4.6 left side the deuteron band is barely visible. As the overlap happens mainly with punch through particles, looking only at the stopped particles improves the

amount of protons cut away. But as the numbers in table 4.1 suggest, there are still about half as many protons as deuterons, since about 0.02% of the protons and 2% of the deuterons remain after cuts. The reason for this is, that a small part of protons appear due to random noise inside the deuteron band of stopped deuterons in some ΔE-E plots. But due to the factor 50 higher cross section, this small part is still a problem. Using the neural net provides a far better ratio of $pp\pi^+$ to $d\pi^+\pi^0$, about 1 proton per 20 deuterons can be expected.

In summary one can say, that the beam energy was so high, that a identification by one ΔE-E plot was not possible, but by using many ΔE-E plots in a neural net a sufficient identification was achieved.

4.2.3. Kinematical fit

For the kinematical fit different input formats for the variables can be chosen. In this case the input format was chosen as energy, mass and angles of particles because the uncertainties are also in these units.

Of the 4 outgoing particles - d, π^+, γ, γ - all 4 are measured, giving 12 measured values. Following particle identification the mass is known and fixed, giving 4 values. Momentum and energy conservation and the mass of the π^0, which decays into the two γs, give another 5 conditions. In this case there would be 5 overconstraints. But many π^+ are punch-through and minimum ionizing, therefore the uncertainty of their energy measurement is large. To avoid losing them, the energy uncertainty for all π^+ is treated as unmeasured. This is acceptable, as 4 overconstraints are still enough.

$$
\begin{aligned}
=> values \quad & 16 \\
masses \quad & -4 \\
E/Pconservation \quad & -4 \\
\pi^0 constraint \quad & -1 \\
measured \quad & -11 \\
& = \\
overconstraints \quad & 4
\end{aligned}
$$

Particle	Uncertainty kinetic energy	Uncertainty θ	Uncertainty Φ
d	10%	1^0	1^0
π^+	unmeasured	1^0	1^0
γ	30%	5^0	5^0
γ	30%	5^0	5^0

Table 4.2.: Uncertainties assumed for kinematical fit

Table 4.2 summarizes the assumed uncertainties. The energy uncertainty of the deuteron is chosen such large because most deuterons have more than 0.3 GeV. But although a big part of the deuterons is punch-through, their energy is still known quite well, because they are not

minimum ionizing. This allows to calculate the real energies from the deposited energies by formulas derived from simulation, where the real deuteron energy is known. A lot of the π^+ are punch through and minimum ionizing, therefore their energy is selected as unmeasured.

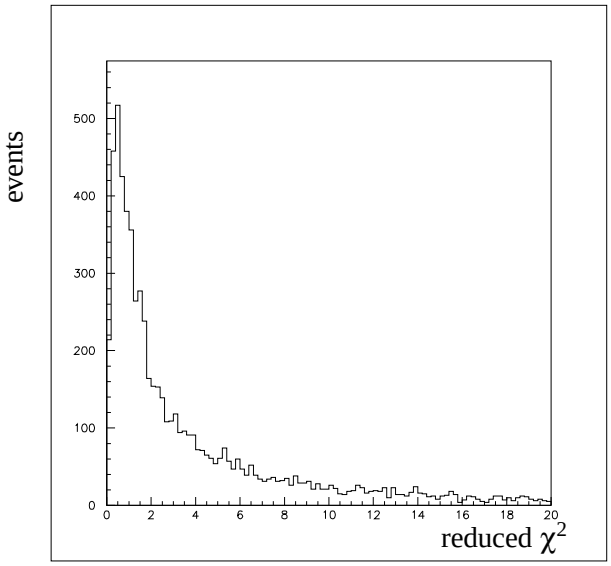

Figure 4.8.: reduced χ^2 for data

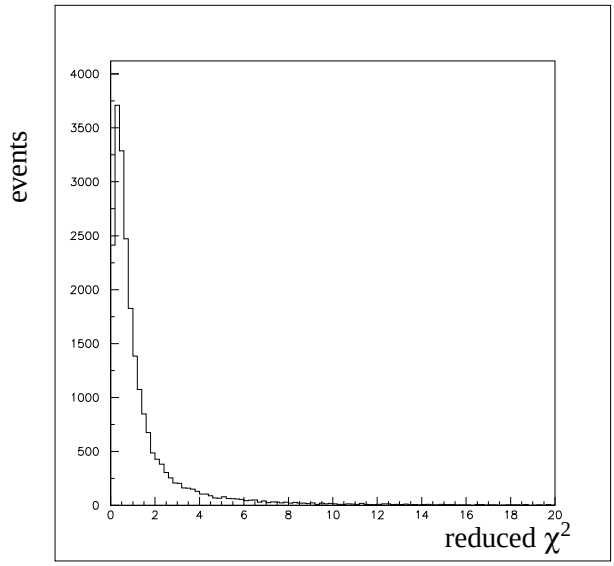

Figure 4.9.: reduced χ^2 for simulation

Figures 4.8 and 4.9 show the reduced χ^2 distributions for model and data. The distribution for the data does not fall off as fast as the one for the model, indicating some background. Therefore a cut was applied. Here $\chi^2 < 6$ was chosen, but other values give similar results, as long as the cut is far enough away from the peak.

Also a kinematical fit is made with proton mass assigned to deuteron and π^+. If the χ^2 of this fit is lower than the fit, where the particles are assumed to be deuteron and π^+, the event is dropped. In simulation this doesn't remove any events, in data this removes about 0.1%.

	before kinfit	after kinfit
data	9277	5068
data with further cut	6676	4462
simulation	22516	21312
simulation with further cut	21226	20187

Table 4.3.: Number of events before and after kinematical fit for $pp \to d\pi^+\pi^0$

The kinematical fit removes a larger percentage of events from data than from simulation. This

indicates that before kinematical fit there is still background in data. To cut away background with kinematical fit is not the best solution, but in this case it is valid. More and tighter cuts could reduce the amount of background before kinematical fit and thereby reduce or eliminate cutting away background with kinematical fit. But the risk would be, to unintentionally cut the data just the way the simulation looks like. This could yield 'results' only dependent upon model and not upon physics.

The numbers shown in Table 4.3 are in favor of using the kinematical fit to cut away background. By applying a cut to the deuteron energy and excluding deposited energies (avoiding using calculated energies) lower than 0.28 GeV or higher than 0.4 GeV the data events for kinematical fit are reduced by one third, but the events after kinematical fit are just reduced by one eighth. This shows, that the kinematical fit mostly removes bad events.

In summary one can say, that $pp \to d\pi^+\pi^0$ was measured rather well and that the problems caused by having both d and π^+ in the Forward Detector could be solved.

4.3. Reaction $pp \to pn\pi^+\pi^0$

This reaction was analysed because it is very similar to $pp \to d\pi^+\pi^0$ in matters of analysis, especially because the same trigger can be used. On the other hand, the physics may or may not be very different, depending upon whether the proton and neutron are in isospin one or isospin zero state. In the latter case the physics would have to be nearly the same as in $d\pi^+\pi^0$.

What is different for the detection of this reaction is the presence of a neutron. Since the neutron can only interact by hadronic interaction with the detectors, the probability to detect the neutron at all is rather low. Detection efficiency for neutrons that pass the detector is in both Forward and Central Detector only about 30%. So the larger part of the neutrons is not detected. Even if the neutron creates a signal, it is difficult to identify it as a neutron signal and also difficult to determine its energy. Since there are 4 particles, not measuring anything of 1 particle leaves the reaction still determined by momentum and energy conservation, if the other 3 particles are fully measured.

Due to this, the solution is to ignore neutrons and actually drop any events, where a possible neutron signal is present. The drawback is, that the π^+ energy has to be measured precisely. Therefore events with punch-through pions have to be ignored.

4.3.1. π^0 identification

As a first step again the requirement of 2 neutral CD tracks and 2 charged FD tracks is set.

The π^0 identification is then exactly the same as in $d\pi^+\pi^0$. Whereas there is some possibility, that the neutron creates a signal in CD and 1 γ is not detected, this is unlikely to cause a misidentification of the neutron as γ, because the energy deposition of neutrons and γs is different in the Central Detector.

Figures 4.10 show the invariant mass spectra of the 2 neutral tracks in the Central Detector for data and model in the region around the π^0 mass, without any further restrictions like energy or number of forward tracks. The π^0 peak is very pronounced.

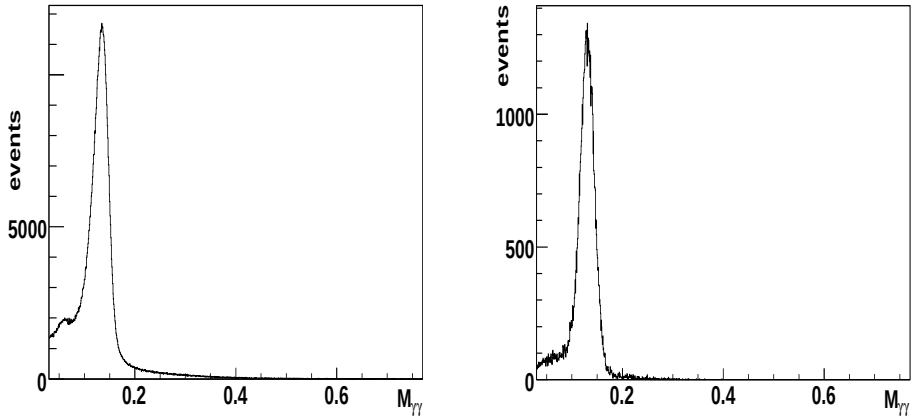

Figure 4.10.: $M_{\gamma\gamma}$, left for data, right for simulation

4.3.2. Proton and π^+ identification

As in $pp \to d\pi^+\pi^0$ the problem in $pp \to pn\pi^+\pi^0$ is again ppπ^0. It is even more severe since both reaction and background have a proton, neither ΔE-E cuts nor neural net can distinguish the reactions using the proton. The pion can be separated by neural net from the second proton, but only if the second proton has sufficiently low kinetic energy.

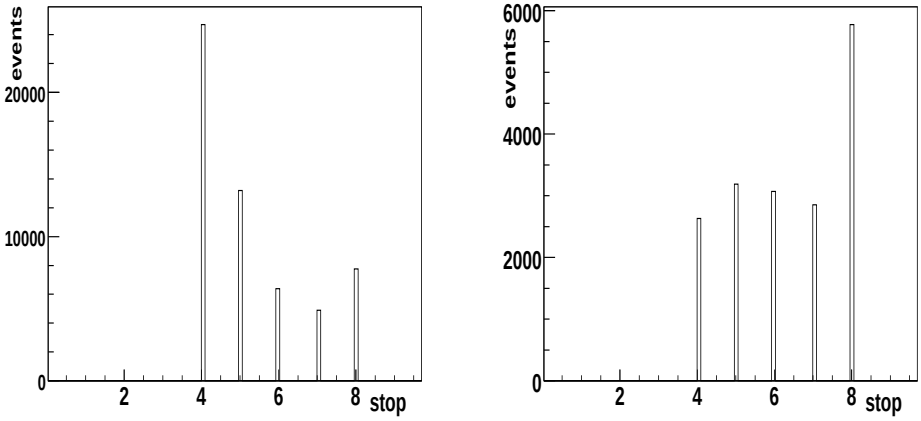

Figure 4.11.: Stop plane of proton left for data, right for simulation, , 4-7 are stopped in first to fourth layer of the Forward Range Hodoscope, 8 is stopped in the Forward Veto Hodoscope, Neural Net already applied

The consequence of this can be seen in Figures 4.11. Even with the very powerful Neural Net already applied, the distribution of stopping layers are very different between simulation and data. As stopping in the 4th layer, which is the first layer of the Forward Range Hodoscope, is

only possible with small kinetic energy, the kinetic energy distributions should be very different.

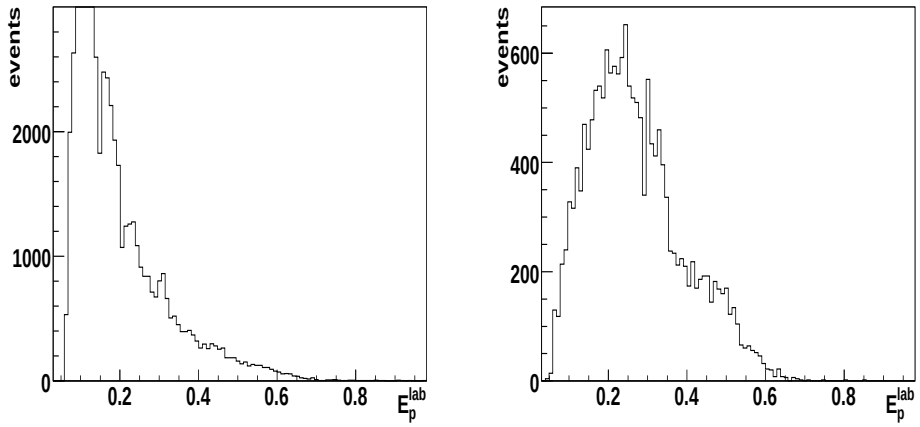

Figure 4.12.: E_{kin}^{lab} of proton, left for data, right for simulation

The effect is clearly visible in figures 4.12. In data there are - compared to model - far too many low energetic protons.

The reason is, that if a proton from ppπ^0 is high energetic, it cannot be distinguished from a π^+. Neural net identifies some part of these as a proton. The other proton then has a lower energy due to kinematics and is stopped in one of the layers closer to the target.

From the simulation it is visible, that the real reaction should have roughly about twice more punch-through protons (the peak at 8 in figure 4.11, left), than are stopped in a single layer (the other peaks in figure 4.11, right). Since in the data the number of protons stopped in first range layer is three or four times higher than the number of punch-through protons, over 80% of these stopped in first layer of the Forward Range Hodoscope are likely to be background.

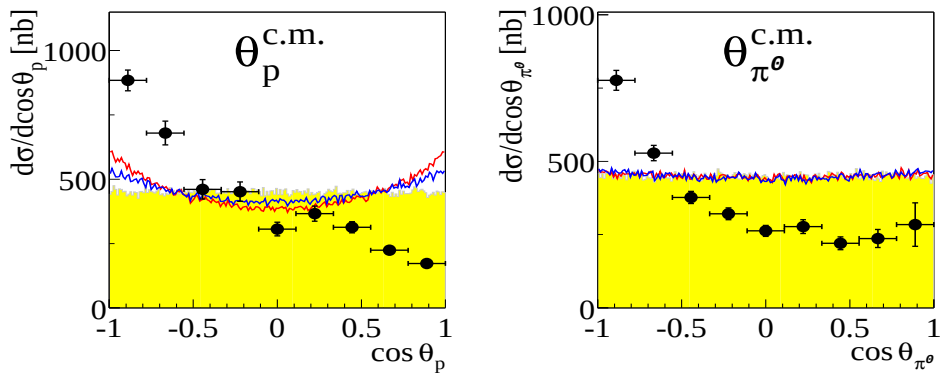

Figure 4.13.: right θ_p^{cm}, left $\theta_{\pi^0}^{cm}$, yellow area phase space, red curve is t-channel $\Delta\Delta$ calculations, blue curve is t-channel $\Delta\Delta$ with $\Sigma \cdot (k_1 \times k_2)$, see section 5.2

This background is so high, that a kinematical fit, which is anyway rather strained due to having an unmeasured neutron, is unable to remove the background.

As Figures 4.13 show, there is after kinematical fit and efficiency and acceptance correction an asymmetry in both π^0 and proton center of mass angle. The enhancement of backward going protons reflects the abundance of low energy protons.

This background can be reduced only with severe cuts. One is to remove punch through pions. This has to be done since any punch through proton is nearly indistinguishable from π^+. Another step is to use several cuts on invariant and missing masses, which seem promising from comparison of simulated $pp\pi^0$ and $pn\pi^+\pi^0$.

But what cannot be avoided is to simply cut away the first 2 layers, where so much background is.

p	π^+	γ
NN identifies p	NN identifies π^+	$E_{SE} > 0$
$\theta < 17^\circ$	$\theta < 17^\circ$	$\theta > 20^\circ$
$E_{FRH3} > 0$	$0.09 < M_{\gamma\gamma} < 0.19$	
	$E_{FRH1} < 0.039$	$E_{PSB} <= 0$
	$E_{FRH2} > 0.019$	
	$MM_{p\pi^+} > 0.95$	
	$MM_{\gamma\gamma} > 1.9$	
	$MM_{p\gamma} > 1$	
	$MM_{p\gamma\gamma} > 0.9$	
	$M_{\pi^+\gamma\gamma} < 0.45$	
	$\theta_n^{lab} > 15^\circ$	
	$\theta_{\pi^0}^{lab} > 45^\circ$	
	$0.12 < E_{\pi^+}^{lab} < 0.27$	
	$E_N^{lab} > 0.27$	
	$E_{\pi^+}^{lab} > 15^\circ$	

Table 4.4.: cuts for $pn\pi^+\pi^0$

Figure 4.14 shows the improvement. Apart from low statistics now the pion center of mass angle is symmetric and the proton center of mass angle is nearly symmetric.

Unfortunately the neutron center of mass angle is still not symmetric after these cuts, therefore further cuts especially on neutron and π^0 angle and energies are necessary.

Particle	Uncertainty kinetic energy	Uncertainty θ	Uncertainty Φ
p	10%	1^0	1^0
n	unmeasured	unm.	unm.
π^+	10%	1^0	1^0
π^0	10%	5^0	5^0

Table 4.5.: Uncertainties assumed for kinematical fit

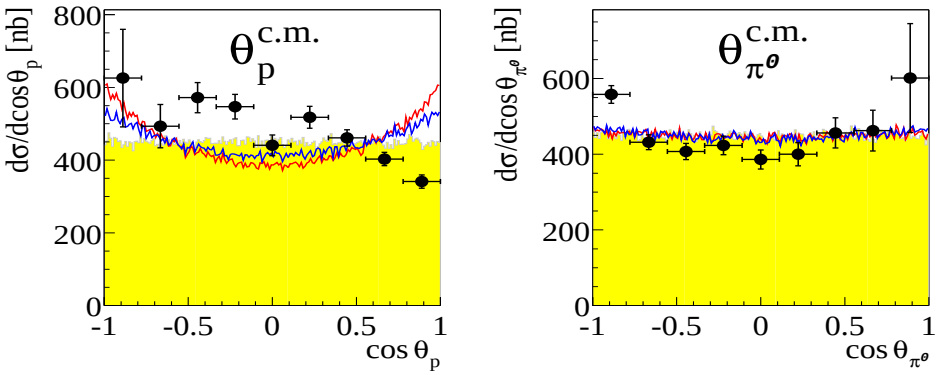

Figure 4.14.: θ_p^{cm} right and $\theta_{\pi^0}^{cm}$ left after dropping particles stopped in first two layers of FRH, curves same as in Fig. 4.13

4.3.3. Kinematical fit

In case of pn$\pi^+\pi^0$ only 4 of the 5 outgoing particles are measured. Apart from these 16 measured values, momentum, energy conservation and the mass of the π^0, which decays into the two γs, give another 5 conditions. Since there are 20 values, this leaves only 1 overconstraint. Therefore punch through π^+ had to be excluded, because without overconstraints, the kinematical fit would not do anything. Table 4.5 shows the assumed uncertainties.

As there is only 1 overconstraint, kinematical fit cannot be used for removing background. The percentage removed due to kinematical fit is nearly the same for data and simulation. χ^2 distributions 4.15 and 4.16 are nearly identical for model and data. So no cut on χ^2 is possible, that would remove a lot of background and little of pn$\pi^+\pi^0$.

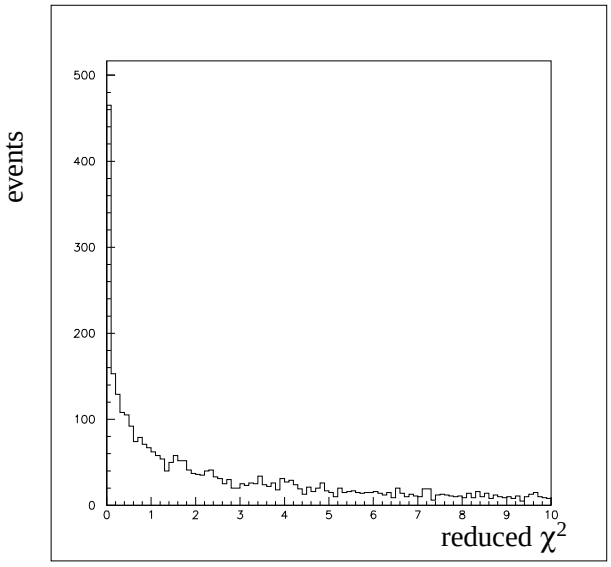

Figure 4.15.: data reduced χ^2

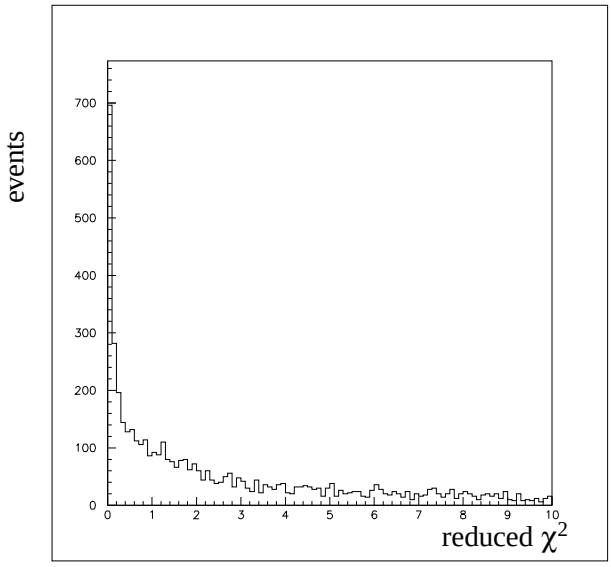

Figure 4.16.: simulation reduced χ^2

5. Results

5.1. Definition of Observables

The results are presented in terms of kinetic energy, scattering angle θ , azimuthal angle ϕ and invariant mass.

The z-axis is in beam direction and the polar scattering angle θ of a track is the angle between the track and the z-axis.

The azimuthal angle ϕ is the angle between the x-axis and the projection of a track to the x-y plane.

The opening angle δ is the angle between two tracks.

The planarity Δϕ is the difference in opening between the ϕ of two tracks.

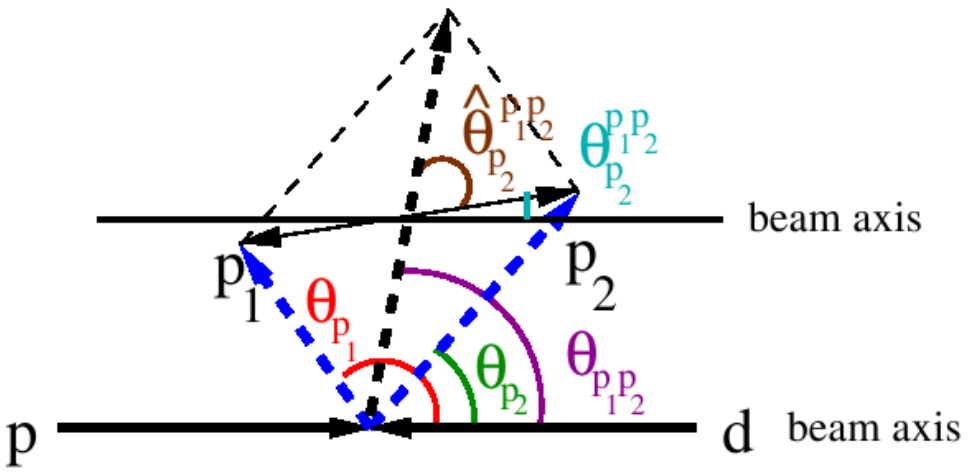

Figure 5.1.: different scattering angles in the subsystem of two particles with 3-momentum vectors p_1 and p_2

Fig. 5.1 shows angles in some subsystems, for which also differential cross sections are shown. The angle $\theta_{p_1p_2}$ is simply the θ angle of the sum vector of $\overrightarrow{p_1}$ and $\overrightarrow{p_2}$. The angle $\theta_{p_1}^{p_1p_2}$ is the angle between $\overrightarrow{p_1}$ and the z-axis in the p_1p_2 subsystem. The angle $\hat{\theta}_{p_1}^{p_1p_2}$ is the angle between $\overrightarrow{p_1}$ and the sum vector in the p_1p_2 subsystem.

The invariant mass is defined as:

$M^2 = (\sum_i E_i)^2 - (\sum_i \vec{p_i})^2$

where E denotes the total energy of particle i and $\vec{p}$ the momentum vector of particle i. Invariant masses are useful, because any decaying particle shows up as peak in the invariant mass of its decay products. The same way also resonances are visible in a invariant mass distribution.

A so called Dalitz plot depicts one invariant mass squared versus another invariant mass squared. It contains information about the relation between the mechanisms, that cause the peaks in the individual invariant mass plots. E.g. decaying particles, that can be produced independently would lead to a different Dalitz plot than particles, that only appear together in the reaction products.

5.2. Theoretical models

As already mentioned in Chapter 1 Risser and Shuster first described the ABC effect by a t-channel ΔΔ excitation (Ref. [7]). In the model a pion exchange leads to the formation of two Δs, which then decay both into nucleon and pion. The two nucleons fuse to a deuteron. Fig. 5.2 shows the corresponding graph.

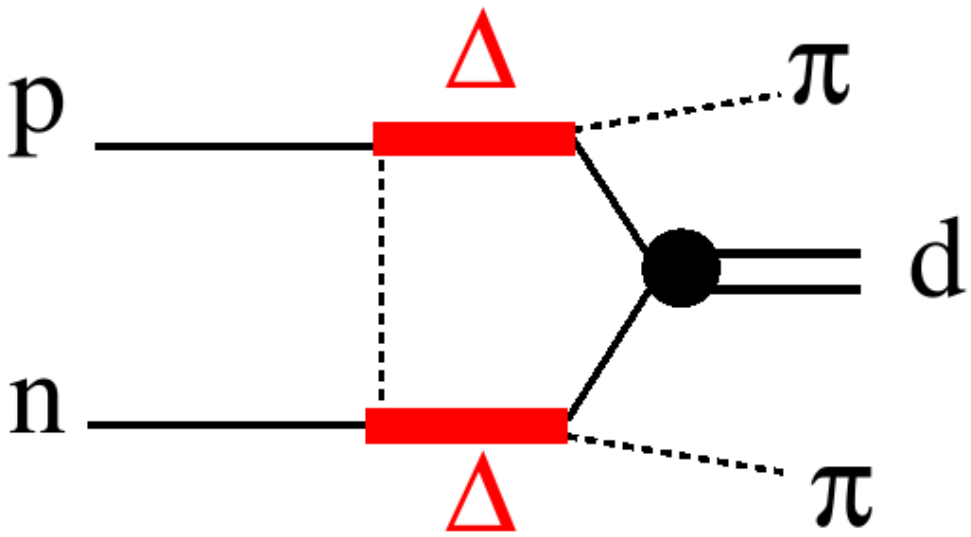

Figure 5.2.: Double-pionic fusion process via t-channel ΔΔ excitation in the intermediate state for the reaction $pn \rightarrow d\pi^+\pi^0$ (Identical to Fig. 1.2)

This t-channel ΔΔ gives a modification of phase space by the factor:

$$|\Delta_1|^2 \cdot |\Delta_2|^2 \cdot |\Pi|^2$$

with the squared pion propagator:

$$|\Pi|^2 = \frac{1}{(q^2 - M_\pi^2)^2}$$

and the squared Δ propagators:

$$|\Delta|^2 = \frac{\Gamma^2/(P_\pi^{d\pi})^2}{(M^2_{\frac{d}{2}\pi} - M_\Delta^2)^2 + (M_\Delta \cdot \Gamma)^2}$$

q is the momentum transfer and $P_\pi^{d\pi}$ is the π momentum in the Δ system. The symbol $\frac{d}{2}$ signals that the particle was assumed to have half the deuteron mass and half the deuteron momentum.

The width Γ according to Risser and Shuster is:

$$\Gamma = \gamma \cdot \frac{R^2 \cdot (P_\pi^{d\pi})^2}{1 + R^2 \cdot (P_\pi^{d\pi})^2}$$

with $\gamma = 0.74$ and $R = 6.3 c/GeV$ as given by Pilkuhn [20].

The essential difference of the $pp \to d\pi^+\pi^0$ reaction to other $\Delta\Delta$ channels e.g. $pn \to d\pi^0\pi^0$ is due to isospin. The isospin of the initial proton pair is 1. The isospin of the deuteron is 0. Therefore the pion pair has isospin 1. In $pn \to d\pi^0\pi^0$ the pion pair has isospin 0, which allows the pions to be in relative s-wave or d-wave. In the isovector channel the pion pair has to be in relative p-wave(ρ channel) due to Bose-symmetry. As shown in Ref. [21] and [22] this is accomplished best by a spin flip with the operator $\vec{\sigma} \cdot (\widehat{k_1} \times \widehat{k_2})$. $\vec{\sigma}$ is the Pauli nucleon-spin operator and $\widehat{k_1}$, $\widehat{k_2}$ are the pion momenta directions.

Another possibility is, that the pions are not only in relative s-wave, but also interact to form a real ρ with the squared propagator:

$$|\rho|^2 = \frac{1}{(M_{\pi\pi} - M_\rho)^2 + (\frac{\Gamma_\rho}{2})^2}$$

The phase space modification used in this work to represent the $\Delta\Delta$ process is:

$$|\Delta_1|^2 \cdot |\Delta_2|^2 \cdot |\Pi|^2 \cdot (\widehat{k_1} \times \widehat{k_2})(\cdot |\rho|^2)$$

where the use of the ρ-propagator is optional.

For $pp \to pn\pi^+\pi^0$ similar models were used.

5.3. Normalization

There are two ways to determine the total cross section. The absolute normalization requires the knowledge of the integrated luminosity, the data acquisition life time and the real acceptance. This complicated method can be avoided by a relative normalization using a reaction with known

cross section. For this purpose of relative normalization the reaction $pp \to pp\pi^0$ was chosen. This avoids all problems from total cross section determination, that arise from the detector or from the data acquisition system, because ppπ^0 is measured with the same trigger as d$\pi^+\pi^0$. To check, whether $pp \to pp\pi^0$ was measured correctly, we exploit that a model with Δ excitation by pion exchange is known to describe the reaction well. From the agreement of that model with our data (see Fig. 5.3) we conclude that our data are sufficiently accurate.

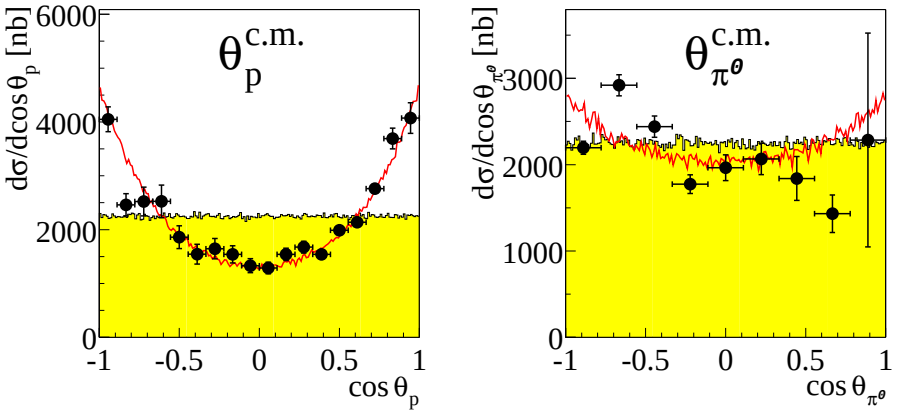

Figure 5.3.: θ_p^{cm} and $\theta_{\pi^0}^{cm}$ for the reaction $pp \to pp\pi^0$, red line shows calculation for t-channel single Δ excitation, yellow area is phase space

5.4. Reaction $pp \to d\pi^+\pi^0$

5.4.1. Differential cross sections

Figures 5.4 - 5.9 show the differential cross sections results for $pp \to d\pi^+\pi^0$. The event selection is described in chapter 4. The solid dots are data points with statistical error bars, the yellow shaded area is phase space, the red dotted curves are t-channel $\Delta\Delta$ calculations, the blue solid line is the same calculation assuming spin flip via $\vec{\sigma} \cdot (\hat{k_1} \times \hat{k_2})$ added and the green dashed curve is a calculation with ρ production (see section 5.2). For the Dalitz plots t-channel $\Delta\Delta$ calculations assuming spin flip via $\vec{\sigma} \cdot (\hat{k_1} \times \hat{k_2})$ were used. For definition of observables see chapter 5.1.

5.4.1.1. invariant masses

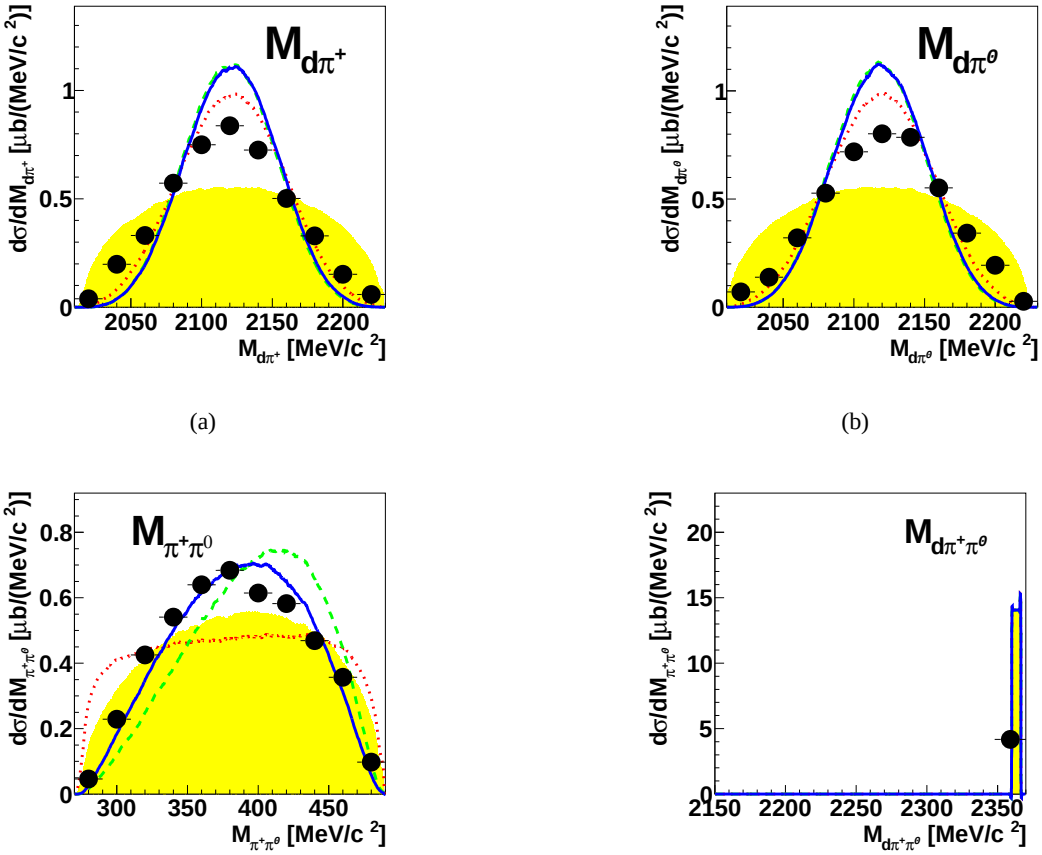

Figure 5.4.: invariant mass spectra for (a) $d\pi^+$, (b) $d\pi^0$, (c) $\pi^+\pi^0$ and (d) $d\pi^+\pi^0$ for the reaction $pp \rightarrow d\pi^+\pi^0$

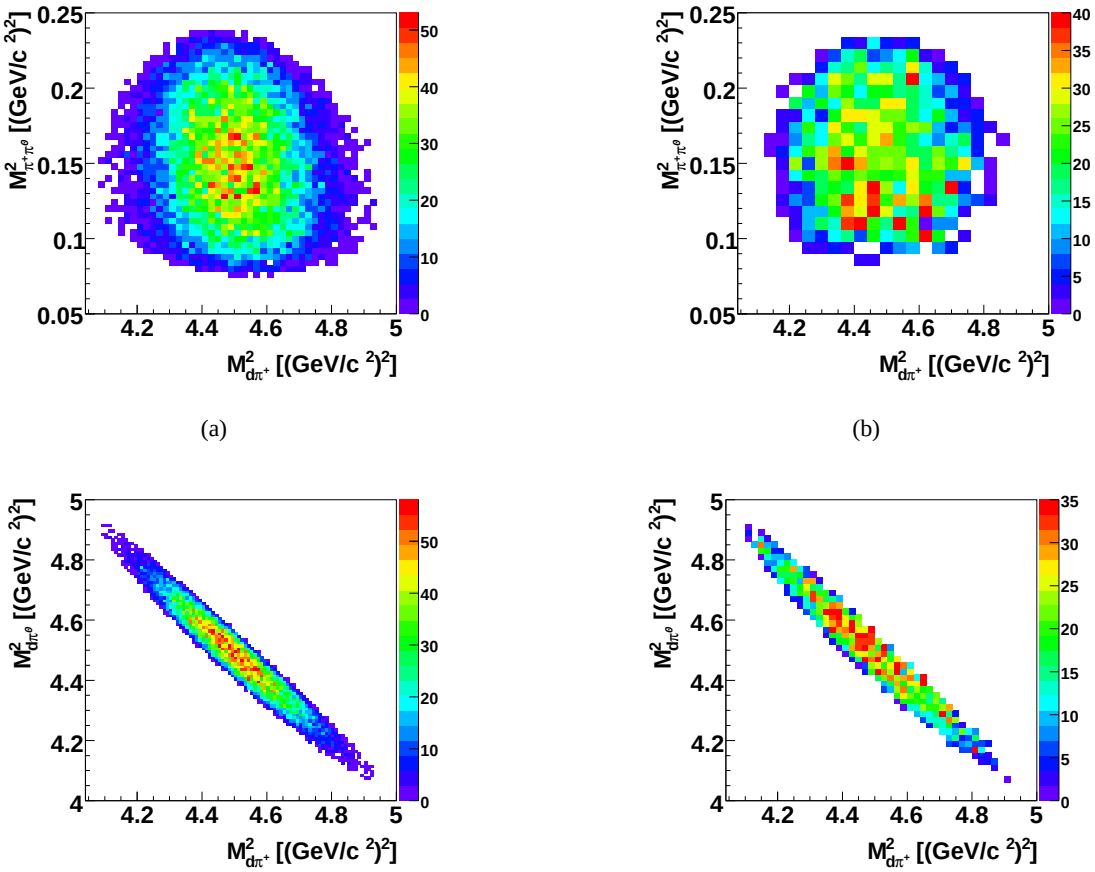

(a) (b)

(c) (d)

Figure 5.5.: Dalitz plot $M^2_{d\pi^+}$ vs $M^2_{\pi^0\pi^+}$ for simulation (a) and data (b) as well as Dalitz plot $M^2_{d\pi^+}$ vs $M^2_{d\pi^0}$ for simulation (c) and data (d) for the reaction $pp \rightarrow d\pi^+\pi^0$

5.4.1.2. energy distributions

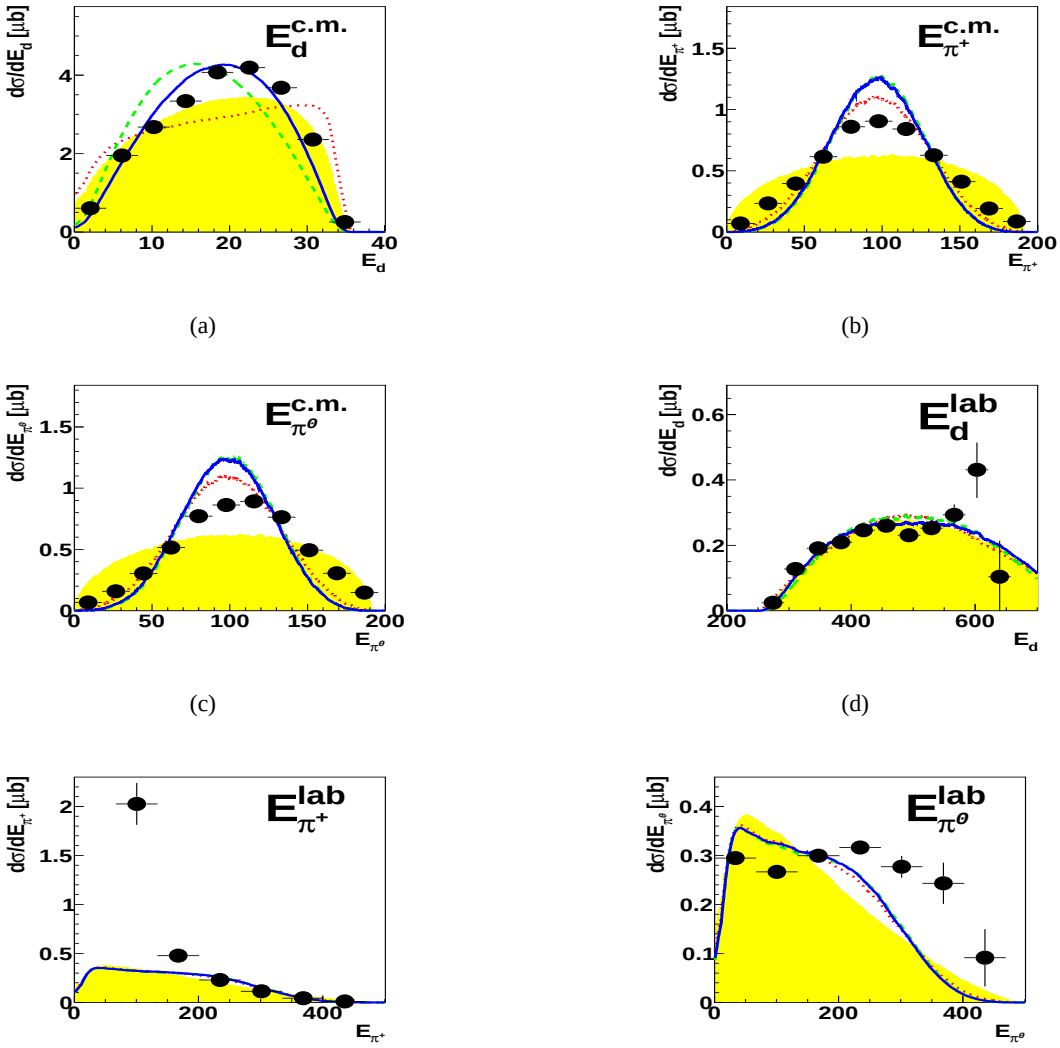

Figure 5.6.: E_{kin} distributions in overall center of mass system for deuteron (a), π^+ (b) and π^0 (c), E_{kin} distribution in lab system for deuteron (d), π^+ (e) and π^0 (f) for the reaction $pp \rightarrow d\pi^+\pi^0$

5.4.1.3. angular distributions

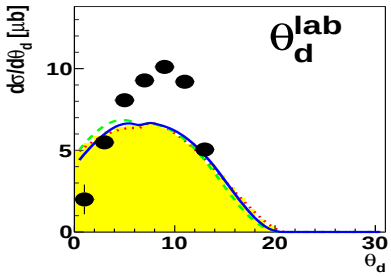

(a)

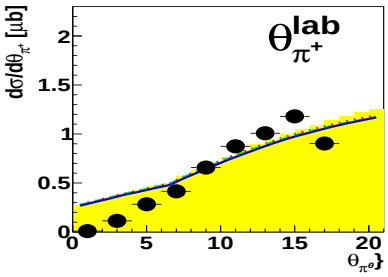

(b)

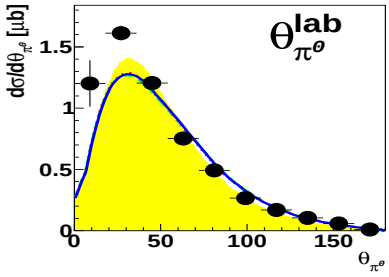

(c)

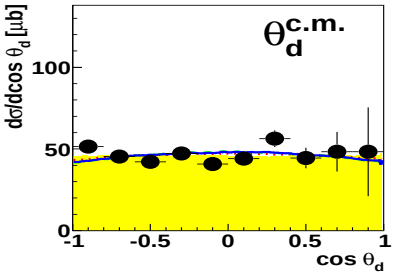

(d)

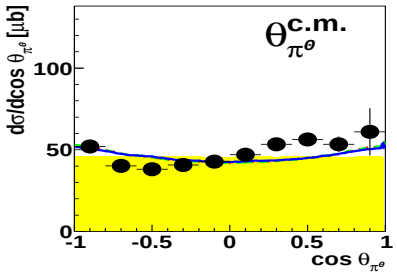

(e)

Figure 5.7.: θ distributions in lab system for deuteron (a), π^+ (b) and π^0 (c) , θ distributions in overall center of mass system for deuteron (d), π^0 (e) for the reaction $pp \rightarrow d\pi^+\pi^0$

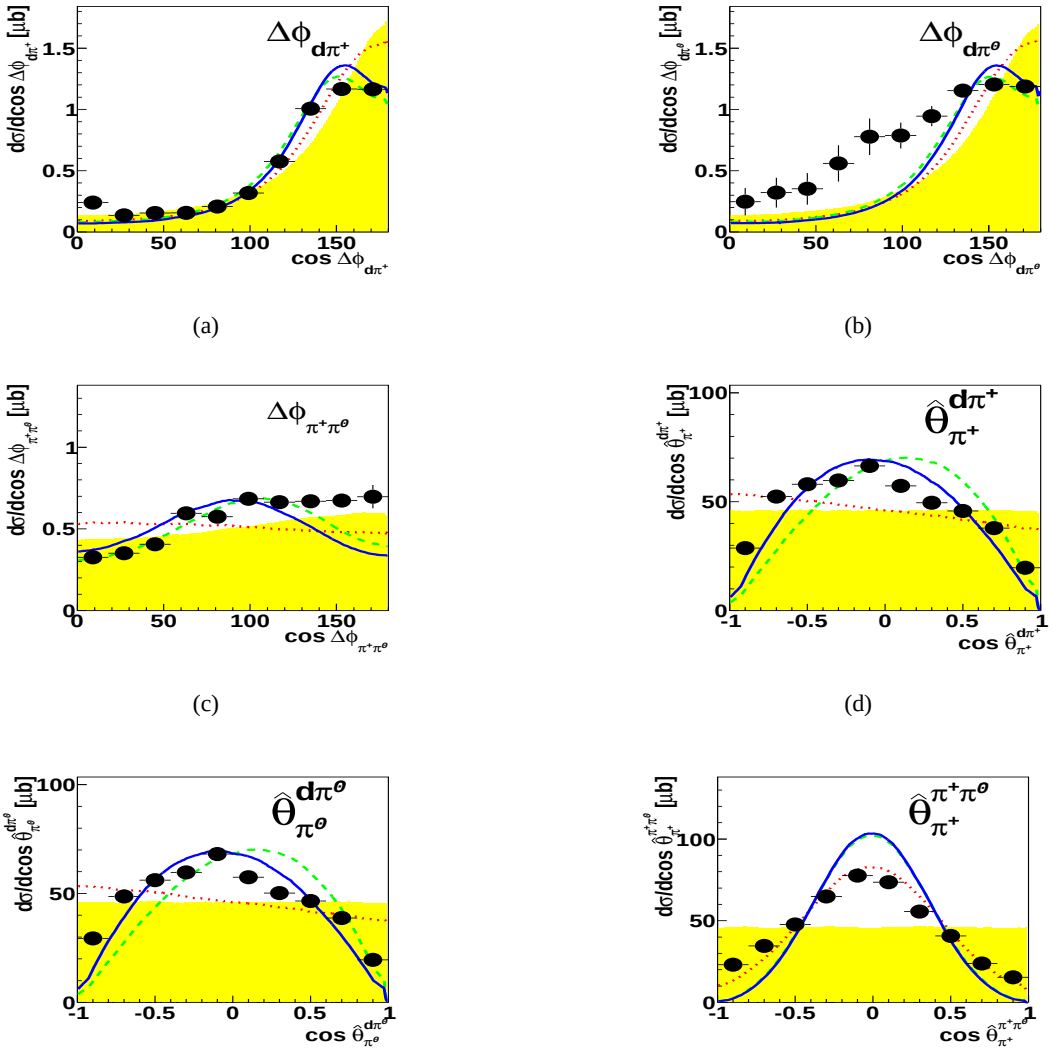

Figure 5.8.: $\Delta\Phi$ distribution of $d\pi^+$ (a), $d\pi^0$ (b) and $\pi^+\pi^0$ (c), angle between track and sumvector in subsystem of π^+ in $d\pi^+$ subsystem (d), π^0 in $d\pi^0$ subsystem (e) and π^+ in $\pi^+\pi^0$ subsystem (f) for the reaction $pp \to d\pi^+\pi^0$

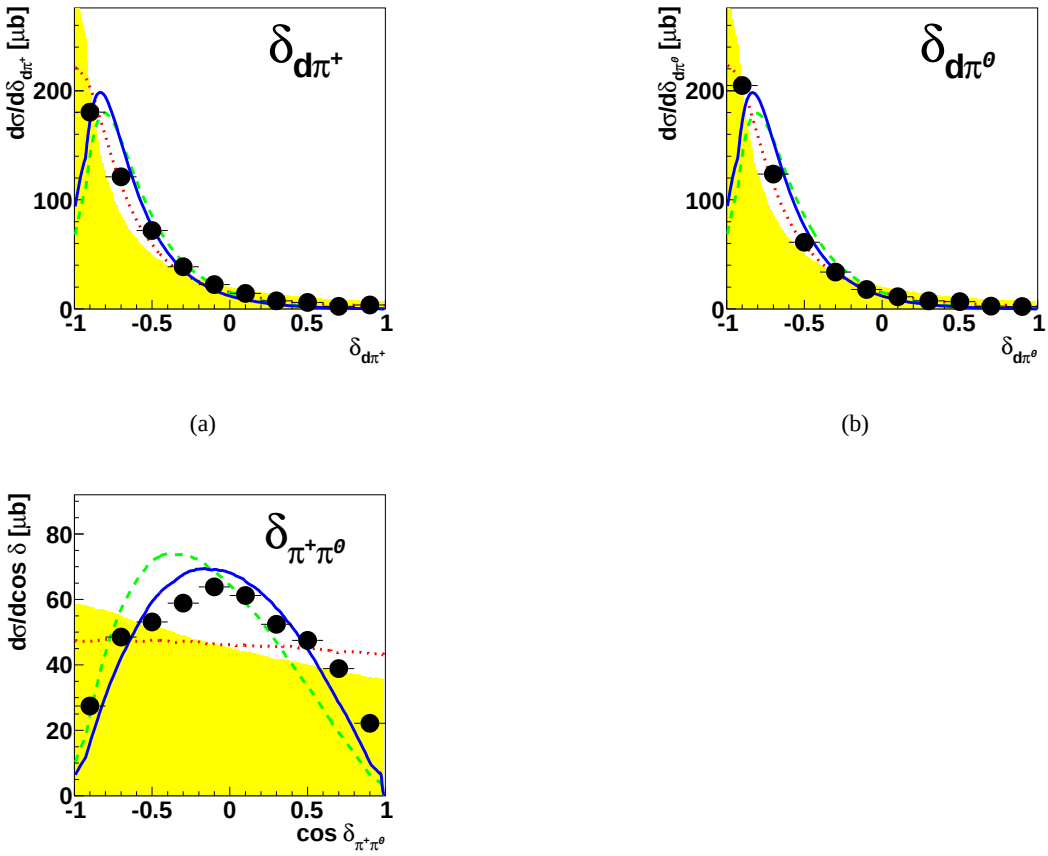

Figure 5.9.: Opening angle in overall center of mass system between (a) deuteron and π^+ (b) deuteron and π^0 (c) π^+ and π^0 for the reaction $pp \rightarrow d\pi^+\pi^0$

5.4.2. Discussion of results for $d\pi^+\pi^0$

Due to the serious problems in trigger selection, the question whether the selection is good, is most important. Suggested by the problems with π^+ in the central detector symmetric angular distributions in the center of mass frame are crucial. These have to be symmetric because the entrance channel is symmetric.

Both Figures 5.7(d) and 5.7(e) are reasonably symmetric and compared with Figures 4.2(a) and 4.2(b) it is obvious, that the chosen selection with π^+ in forward detector avoids such serious defects.

The other partial differential cross sections are described well by a simulation using t-channel $\Delta\Delta$ excitation assuming a spin flip. As a small deficiency, high energetic π^0 with small scattering angle are pronounced in respect to simulations, which is coupled with fewer high energetic π^+

with small scattering angle (see Figures 5.6 e and f and Figures 5.7 b and c) . But this effect is in phase space regions with little statistical weight. Therefore it is not possible to study this problem further with the selection method. Luckily it does not affect the other distributions in a serious way.

Both nucleon-pion invariant mass spectra (Figures 5.4(b) and 5.4(a)) show a very pronounced peak structure where the Δ excitation is expected. The mass of a Δ is 1.232 GeV and it decays into a proton or neutron and a pion. So if just a single Δ decays and the decay nucleon fuses with another nucleon to form a deuteron, the invariant mass of the system would be around 1.232 GeV + 0.938 GeV $\approx$ 2.17 GeV, since the momentum of the second nucleon is nearly identical to the nucleon emerging from the Δ.

The Dalitz plots in Fig. 5.5 and its projections, the $M_{d\pi^+}$ and $M_{d\pi^0}$ spectra, show that both peak structures in the invariant mass spectra appear simultaneously.

This indicates $\Delta\Delta$ excitation. As described in section 5.2 the t-channel ansatz of Risser and Shuster gives a description of the process with a pion exchange, two Δ propagators and the fusion of the two nuclei to deuteron. This ansatz, shown as red dotted curve in distributions, describes the nucleon-pion invariant masses reasonably, but fails with the pion-pion invariant mass and opening angle distribution, Figures 5.4(c) and 5.9(c). In the two pion invariant mass spectrum, this model causes enhancements at low and high invariant masses (theoretical ABC effect), but data do not support this.

The reason is, that the t-channel $\Delta\Delta$ ansatz assumes a s- or d-wave between the two pions. Due to Bose symmetry the wave function of the two pions have to be symmetric. The wave function is composed of a spin part, a isospin part and one for angular momentum. The spin part is symmetric, as both have spin zero. Due to isospin conservation the two pions must have isospin one, as pp has isospin one and the deuteron isospin zero. To have overall symmetric wave functions, the asymmetry in isospin part has to be offset by an asymmetry in angular momentum. Therefore the relative angular momentum of the two pions cannot be even, but has to be odd. So in the $pp \rightarrow d\pi^+\pi^0$ channel the pions cannot be in s- or d- wave, but are most likely in p-wave as the higher odd angular momenta are far less likely to occur. This is best described by a nucleon spin flip. The nucleon spin flip operator σ comes with the term $(\widehat{k_1} \times \widehat{k_2})$. This term enforces a sinus behavior upon the opening angle between the two pions.

As the opening angle distribution of the two pions (Fig. 5.9(c)) shows, this is just what the data look like and the model with the $(\widehat{k_1} \times \widehat{k_2})$ term (blue solid line) describes the data much better. In the invariant mass spectrum of the two pions (Fig. 5.4(c)) this also removes the enhancements in low and high invariant masses in accordance with data. A t-channel $\Delta\Delta$ with a spin flip operator $\vec{\sigma} \cdot (\widehat{k_1} \times \widehat{k_2})$ is in accordance with data.

The assumption, that a real ρ emerges from the pion-pion interaction, is not supported by data. In all spectra, where the model with and without ρ propagator differ, the model without ρ describes data better.

5.4.2.1. ABC effect

The ABC effect as described in Ref. [19] is expected to appear in isoscalar channels and there in particular in invariant masses and opening angle of the pions. ABC would mean a large enhancement at low invariant masses of $\pi^+\pi^0$ and thereby an enhancement at small opening

angles between π^+ and π^0.

Fig. 5.4(c) shows that the invariant mass of $\pi^+\pi^0$ shows no enhancement at low masses reminiscent of the ABC effect.

In the opening angle (Fig. 5.9(c)) the corresponding effects are obvious as well, the pions seldom go parallel or antiparallel. This again shows that no ABC effect is present, since this would require the pions to move in parallel. It also provides further evidence, that the ABC effect cannot be of isovector nature, as isovector channel requires the spin flip term $\sigma(\widehat{k_1} \times \widehat{k_2})$. Such a cross product yields a sine in the opening angle, which as visible from the spectra is incompatible with a low mass enhancement in the invariant mass spectrum of $\pi^+\pi^0$.

5.4.2.2. Total cross section

For the determination of the total cross section the ppπ^0 background is actually of help, since the reaction uses the same trigger and its cross section is known to some extent. Simply by measuring the ppπ^0 from the same runs using the same trigger, correcting the amount for acceptance in both cases and comparing the number of ppπ^0 to the number of d$\pi^+\pi^0$ gives the relative cross section. With the ppπ^0 cross section known one arrives at the d$\pi^+\pi^0$ cross section.

Table 5.2 shows the event numbers for data, simulation and simulation through detector for the two reactions. For the simulation t-channel $\Delta\Delta$ with $\sigma \cdot ((\widehat{k_1}) \times (\widehat{k_2}))$ was used since this describes the data well (solid blue line in differential cross section distributions). The total number of events in all runs is calculated by (data*simulation/simulation through detector). The relative cross section $\sigma_{d\pi^+\pi^0}/\sigma_{pp\pi^0}$ is calculated by (calculated number of events d$\pi^+\pi^0$ / calculated number of events ppπ^0). The total cross cross section is calculated by multiplying the relative cross section with 4.3 - 4.9 mb (Value from [9]). 'less kinfit' denotes the selection, where more cuts are applied before kinematical fit in an attempt to reduce reliance on kinematical fit to cut away bad events (see section 4.2.3).

	d$\pi^+\pi^0$	d$\pi^+\pi^0$ less kinfit	ppπ^0 number of events
data	5068	4462	19110
model	566545	566545	1034259
model through detector	21312	20187	2925
calculated number of events	134724	125225	6757158
$\sigma_{d\pi^+\pi^0}/\sigma_{pp\pi^0}$	0.01993	0.018528	
$\sigma_{d\pi^+\pi^0}$ μb	86-98	80-91	

Table 5.1.: Number of events in d$\pi^+\pi^0$ and ppπ^0 and approximate total cross section of d$\pi^+\pi^0$, lower number assuming $\sigma_{pp\pi^0}$ = 4.3 mb, higher number assuming 4.9 mb

The uncertainty of the ppπ^0 cross section alone gives an error for the d$\pi^+\pi^0$ cross section of 10 μb, this makes any high precision impossible. The uncertainty from the different selection method, in one case more is cut by the kinematical fit in the other case more cuts are made beforehand, is in the order of 6 μb, Together with statistical error this brings the total error to 15μb. Therefore the result for the $pp \to d\pi^+\pi^0$ cross section is

$\sigma_{d\pi^+\pi^0}$ **= 92** $\pm$ **15** μ**b** , $E_{beam} = 1.1GeV$

Note that the result published in [30] is incorrect by a factor of two due to an error in the previous $pp \rightarrow pp\pi^0$ analysis, which caused half of events to be lost.

As a side note this calculation shows, that the ppπ^0 background is really about 50 times more numerous than the d$\pi^+\pi^0$ signal. This shows, that as long as the trigger requires the π^+ to be in an angular region where also protons from ppπ^0 can go, there always would be large problem to get rid of the proton background. Because whatever method or detector is used peaks or bands will have a gaussian distribution and although this could already be small in the area where the pion peak/band is, the factor 50 can change that into a relevant background. The only solution would be to cut for high pion angles where the protons cannot go, but that would reduce statistics. In this respect a 16% error is satisfactory.

5.4.2.3. Effects of different models upon total and differential cross sections

Differing models can give a different energy dependence for the total cross section. Whereas in this work the $pp \rightarrow d\pi^+\pi^0$ cross section was only determined for one energy, there exist other total cross section measurements, mostly bubble chamber data, see Ref. [8] and [9]. The total cross section measured in this work is in good agreement with the previous results.

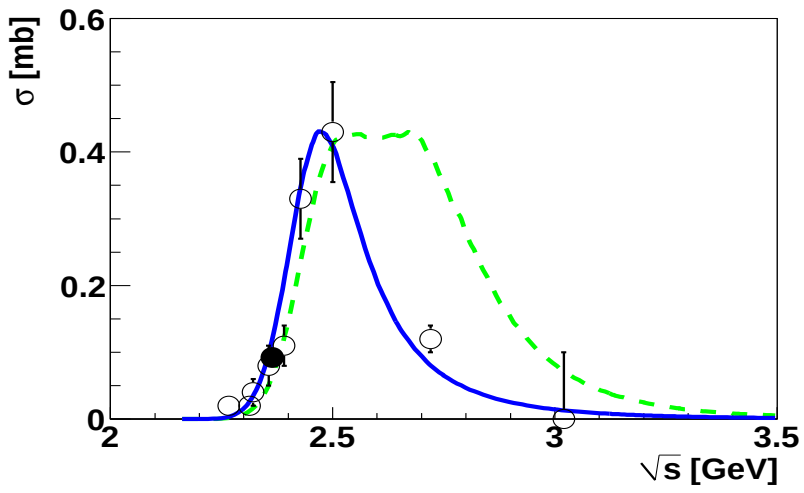

Figure 5.10.: total cross section, blue t-channel $\Delta\Delta$ with $\sigma \cdot ((k_1) \times (k_2))$, green additionally with ρ meson production

Fig. 5.10 shows the total cross section versus the center of mass energy $\sqrt{s}$, with the solid dot from this work and the open dots from Ref. [8] and [9]. The cross section measured in this work confirms the older values.

The blue line shows the expected cross section versus energy behavior for the model without

the formation of a real ρ. The green dashed line shows the same model with a ρ propagator. The old data points confirm, which is also supported by differential cross sections of this work, that the reaction $pp \to d\pi^+\pi^0$ does not excite a ρ.

An interesting problem arises from the width of the Δ. We know it is momentum dependent in principle (Ref. [31]). But there are several suggestions for momentum dependence. The one used here is by Pilkuhn [20] and Risser-Shuster [7] and uses a width proportional to $q^3/(1+R^2q^2)$. Since the cross section is proportional to the width and hence dependent on momentum transfer q, which increases with the center of mass energy, its energy dependence is very sensitive to that of the width.

In Ref. [23] an additional width factor proportional to $(q_0^2 + const)/(q^2 + const)$ has been suggested. This factor ensures, that the width peaks near the resonance pole and then falls off again. Fig. 5.12 shows, that this change in the width has a huge effect upon the total cross section predicted by the model. In this case the model with a real ρ would fit better.

As a first attempt to describe the data in case of Δ excitation a constant width model is often used. But a model with a constant width cannot describe the data. The total cross section can be approximately described with constant width model, except for low energies, where the cross section calculated from a constant width model rises too fast and too soon (see Fig. 5.11).

In the differential cross section a model with constant width fails to describe the data. A t-channel ΔΔ model - so just $|\Delta_1|^2 \cdot |\Delta_2|^2 \cdot |\Pi|^2$ see Chapter 5.2 - should show a Δ excitation in the $d\pi^+$ invariant mass distributions, but the red curve in Fig. 5.13(a) is nearly phase space like. On the other hand the green curve representing the model with a momentum dependent width shows a excitation very similar to data.

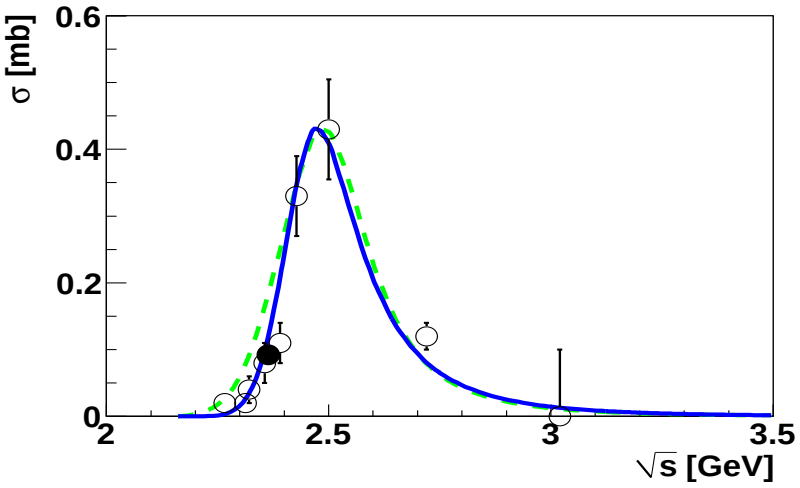

Figure 5.11.: total cross section, blue model with momentum dependent width, green with constant width, both t-channel $\Delta\Delta$ with $\sigma \cdot ((k_1) \times (k_2))$

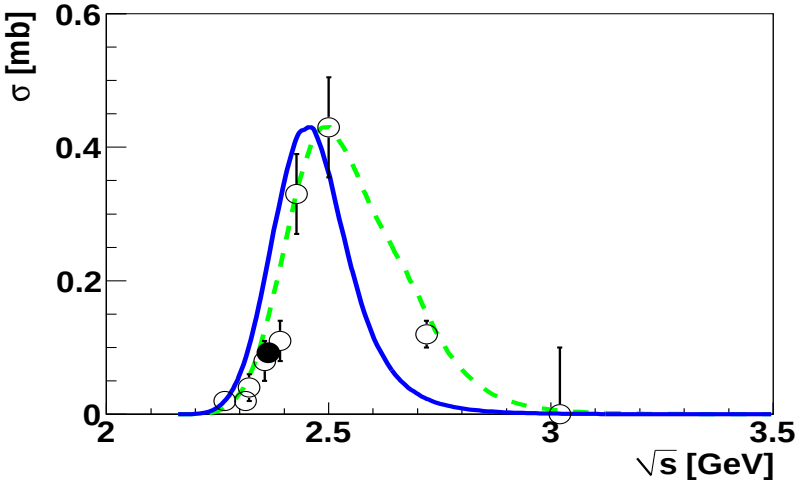

Figure 5.12.: total cross section with additional width factor $(q_0^2 + const)/(q^2 + const)$, blue without and green with ρ meson, both t-channel $\Delta\Delta$ with $\sigma \cdot ((k_1) \times (k_2))$

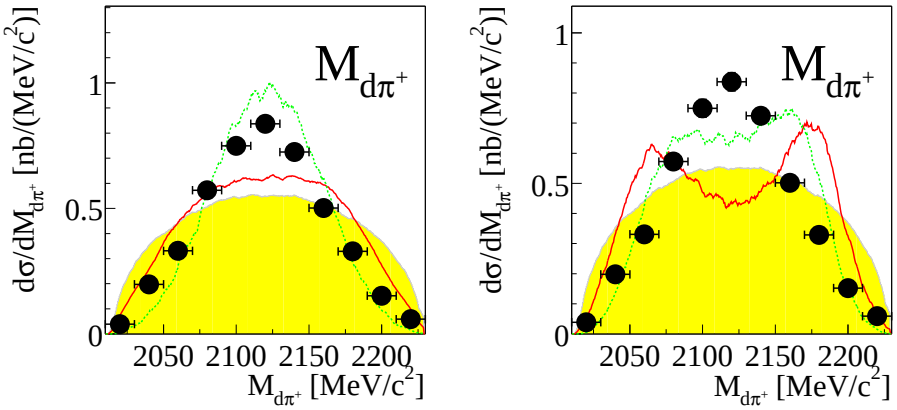

Figure 5.13.: $M_{d\pi^+}$ red line is with constant width, green momentum dependent width both without $\sigma \cdot (\vec{k_1} \times \vec{k_2})$, left width 0.115 GeV , right 0.05 GeV, for momentum dependent width this is the width at the resonance

The problem of a constant width is even more visible, when the width is changed to unphysical values. With a constant width of 0.05 GeV the model predicts a mass distribution with two peaks in sharp contrast to the data (see Fig. 5.13(b)). The reason for this is, that the invariant mass is not the nucleon-pion invariant mass, where both particles can be decay products of the same Δ , but the deuteron-pion invariant mass, where one constituent particle of the deuteron is from one Δ and the other from the other Δ decay.

With a constant width the individual terms of the Δs have a maximum in case of $M^2_{\frac{d}{2}\pi} - M^2_\Delta = 0$. Since the nucleon from the Δ fuses with another nucleon to a deuteron, this corresponds to an invariant mass of deuteron and pion of about $M_{d\pi} = 2.17\frac{GeV}{c^2} \approx 1.232GeV + 0.938GeV$, so in case of very low or zero constant width, a peak is visible at or near that position.

The Dalitz plot 5.14 shows, that due to the fusion to a deuteron the phase space is so limited, that a peak in one invariant mass causes through reflection a peak in the other invariant mass. $M^2_{d\pi^+} \approx 4.7(\frac{GeV}{c^2})^2$ limits the other invariant mass to $M^2_{d\pi^0} \approx 4.3(\frac{GeV}{c^2})^2$. Therefore the peak caused by one Δ term with a low constant width at $M_{d\pi^+} \approx 2.17\frac{GeV}{c^2} = \sqrt{4.7(\frac{GeV}{c^2})^2}$ yields a peak in the other invariant mass at $M_{d\pi^+} \approx 2.07\frac{GeV}{c^2} = \sqrt{4.3(\frac{GeV}{c^2})^2}$.

These two peaks are visible in case of a low enough constant width and even an increase in width cannot change the peak structure so, that they overlap to form the single peak visible in data. Therefore a constant width model only shows a plateau structure and cannot describe the data.

The momentum dependent width model on the other hand shows an enhancement even when the width is reduced by a factor of more than 2.

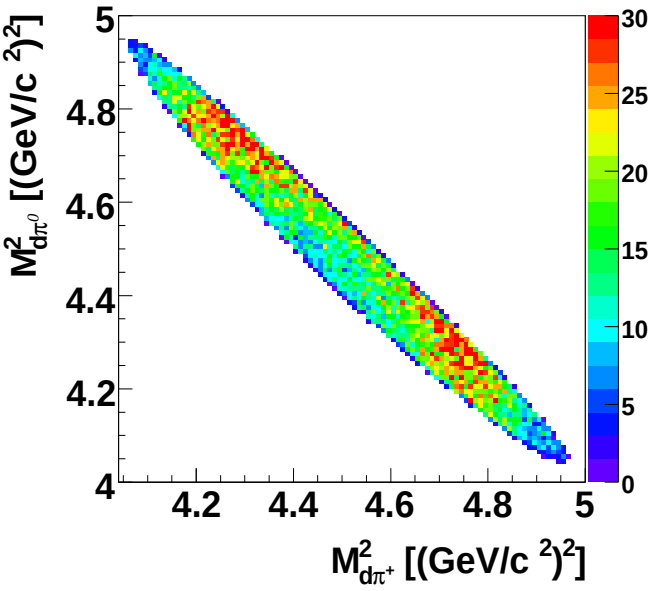

Figure 5.14.: Dalitz plot simulation of ΔΔ with constant width of 0.05 GeV

Simulations for the $pp \to d\pi^+\pi^0$ at higher energies than 1.1 GeV show that such a structure with two peaks appears even in a model with a momentum dependent width. But this only happens at energies, where other reaction mechanisms are far more dominant than ΔΔ production, therefore this structure would not be visible in data.

All these considerations show, that a good model and especially correct description of the Δ width is crucial to describe the data correctly, as even small changes to the width or approximations have large effects on the shape of the model.

5.5. Reaction $pp \to pn\pi^+\pi^0$

5.5.1. Differential cross sections

The following sections show the differential cross sections results for $pp \to pn\pi^+\pi^0$. The event selection is described in chapter 4. The solid dots are data points, the yellow shaded area is phase space, the red curves are t-channel ΔΔ calculations and the blue line is the same except, that a spin flip is assumed via $\sigma \cdot (\widehat{k_1} \times \widehat{k_2})$ (see section 5.2). For definition of observables see chapter 5.1.

5.5.1.1. invariant masses

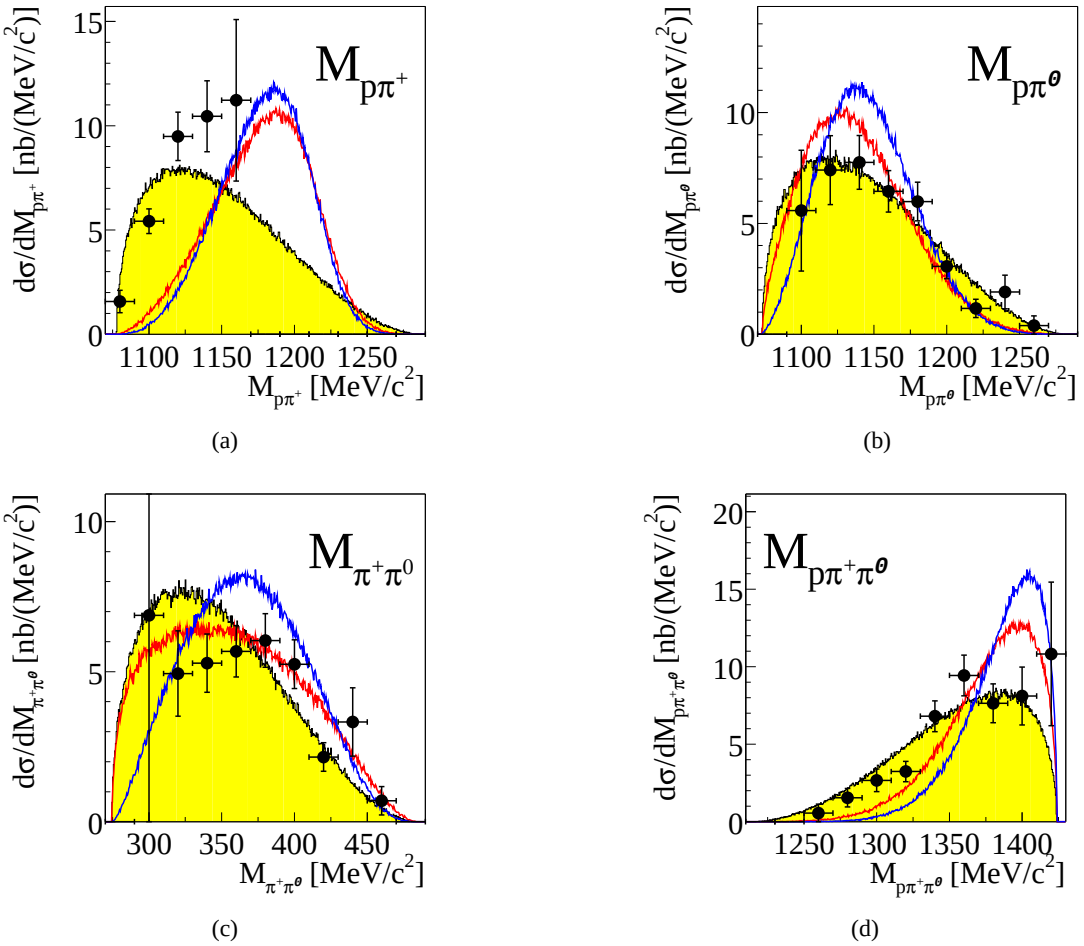

Figure 5.15.: invariant mass spectra for (a) $p\pi^+$, (b) $p\pi^0$, (c) $\pi^+\pi^0$ and (d) $p\pi^+\pi^0$

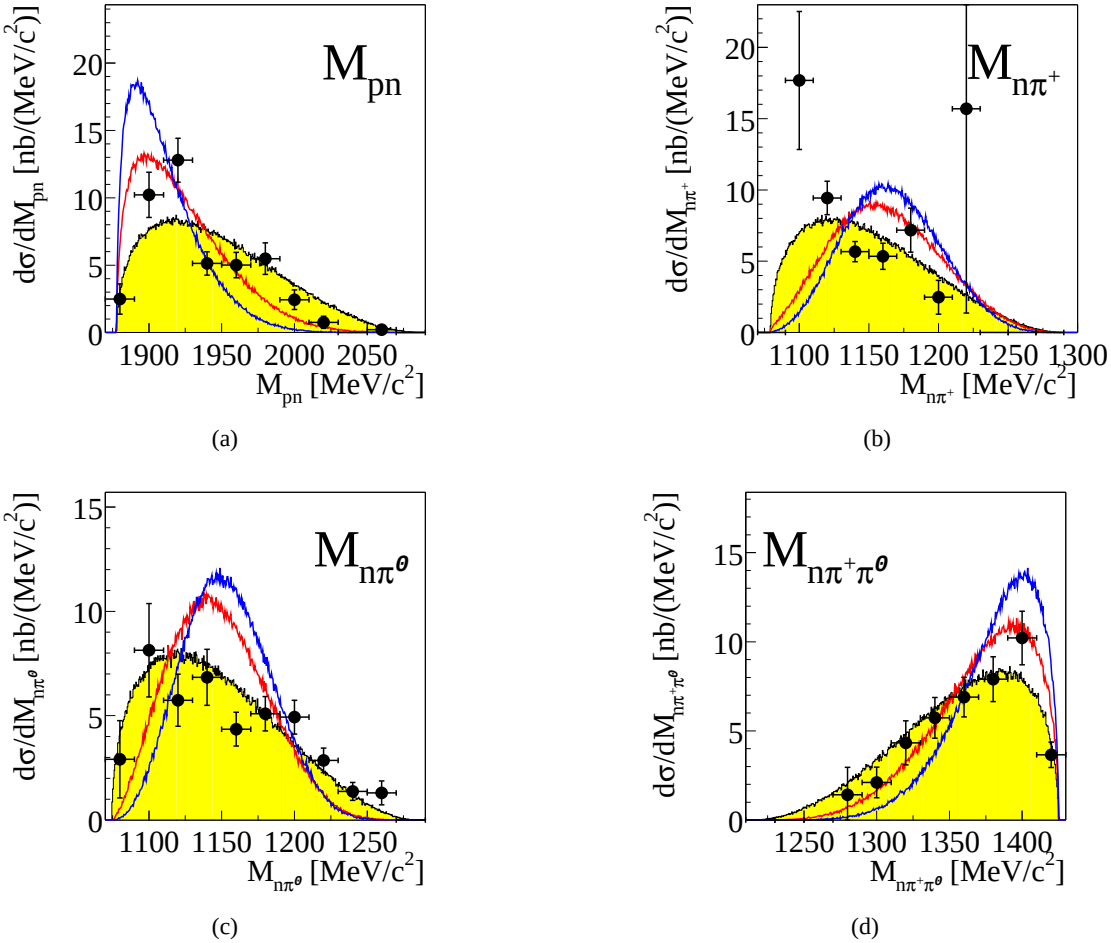

Figure 5.16.: invariant mass spectra for (a) pn, (b) $n\pi^+$, (c) $n\pi^0$ and (d) $n\pi^+\pi^0$

5.5.1.2. energy distributions

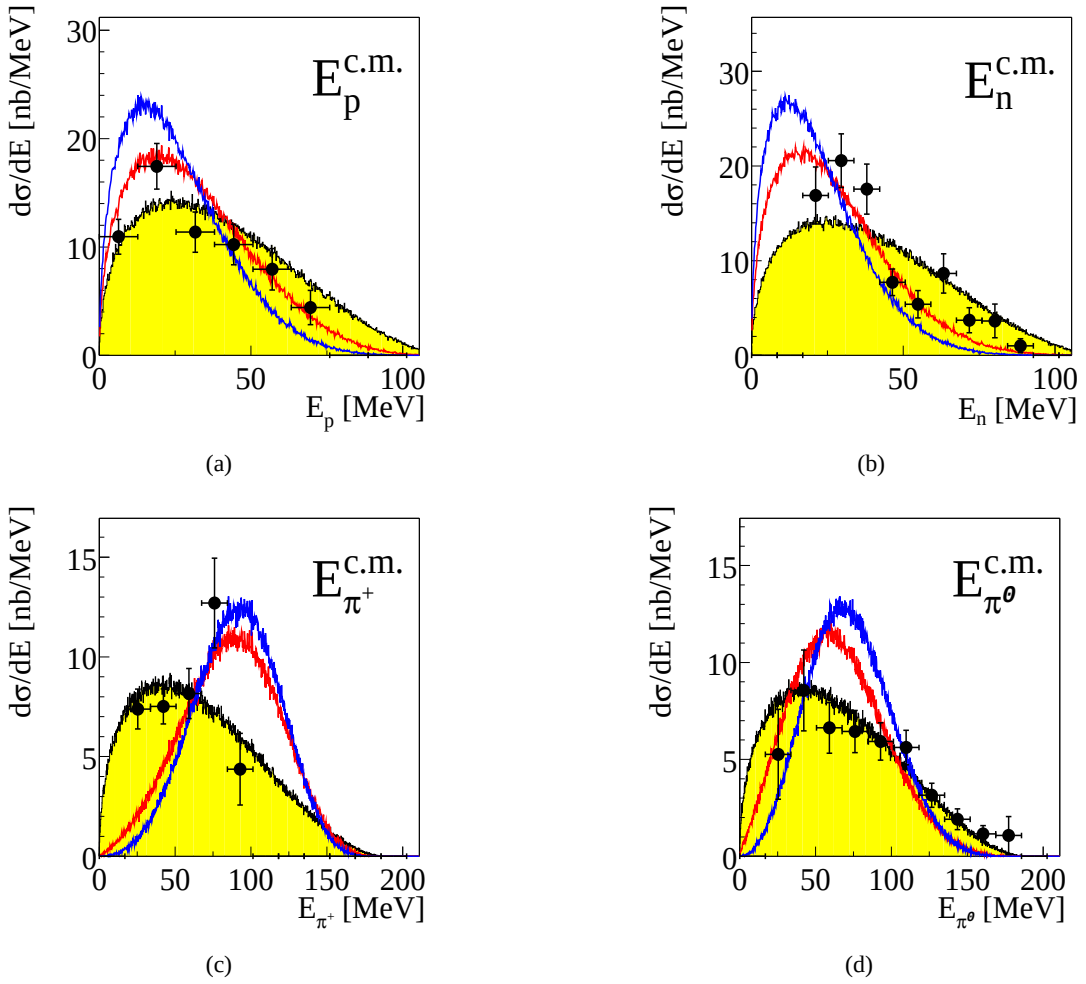

Figure 5.17.: E_{kin} distributions in center of mass system for (a) proton, (b) neutron, (c) π^+ and (d) π^0

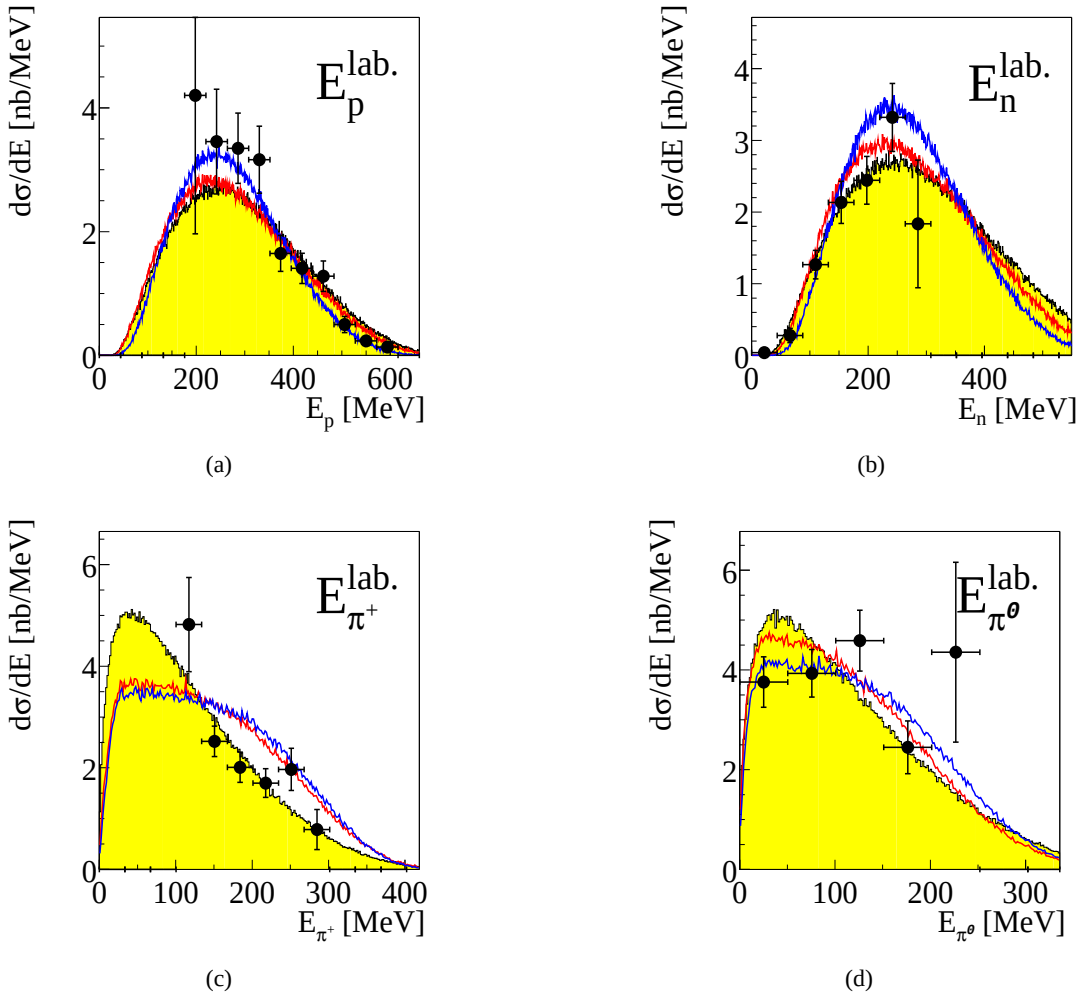

Figure 5.18.: E_{kin} distributions in lab system for (a) proton, (b) neutron, (c) π^+ and (d) π^0

5.5.1.3. angular distributions

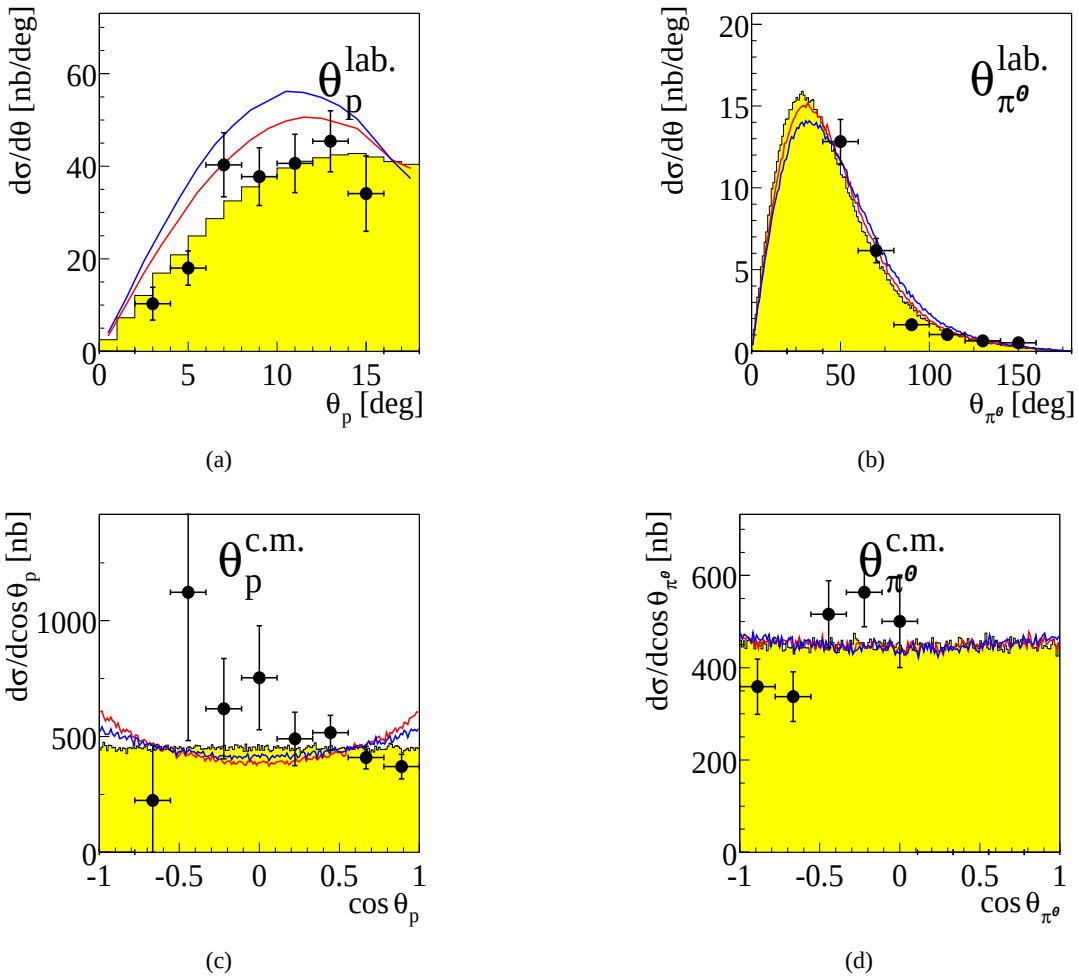

Figure 5.19.: θ distributions in lab system for (a) proton and (b) π^0, θ distributions in center of mass system for (c) proton and (d) π^0

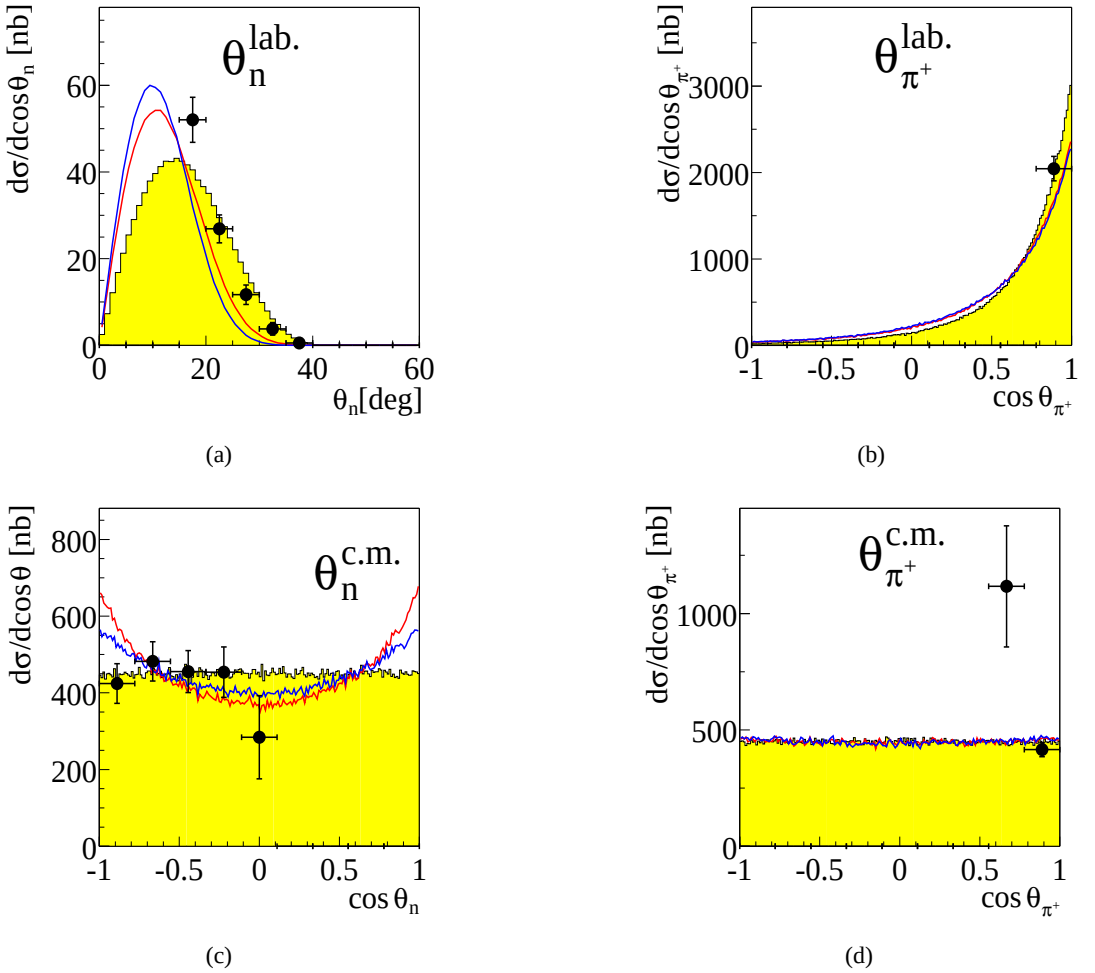

Figure 5.20.: θ distributions in lab system for (a) neutron and (b) π^+ , θ distribution in centre of mass system for (c) neutron and (d) π^+

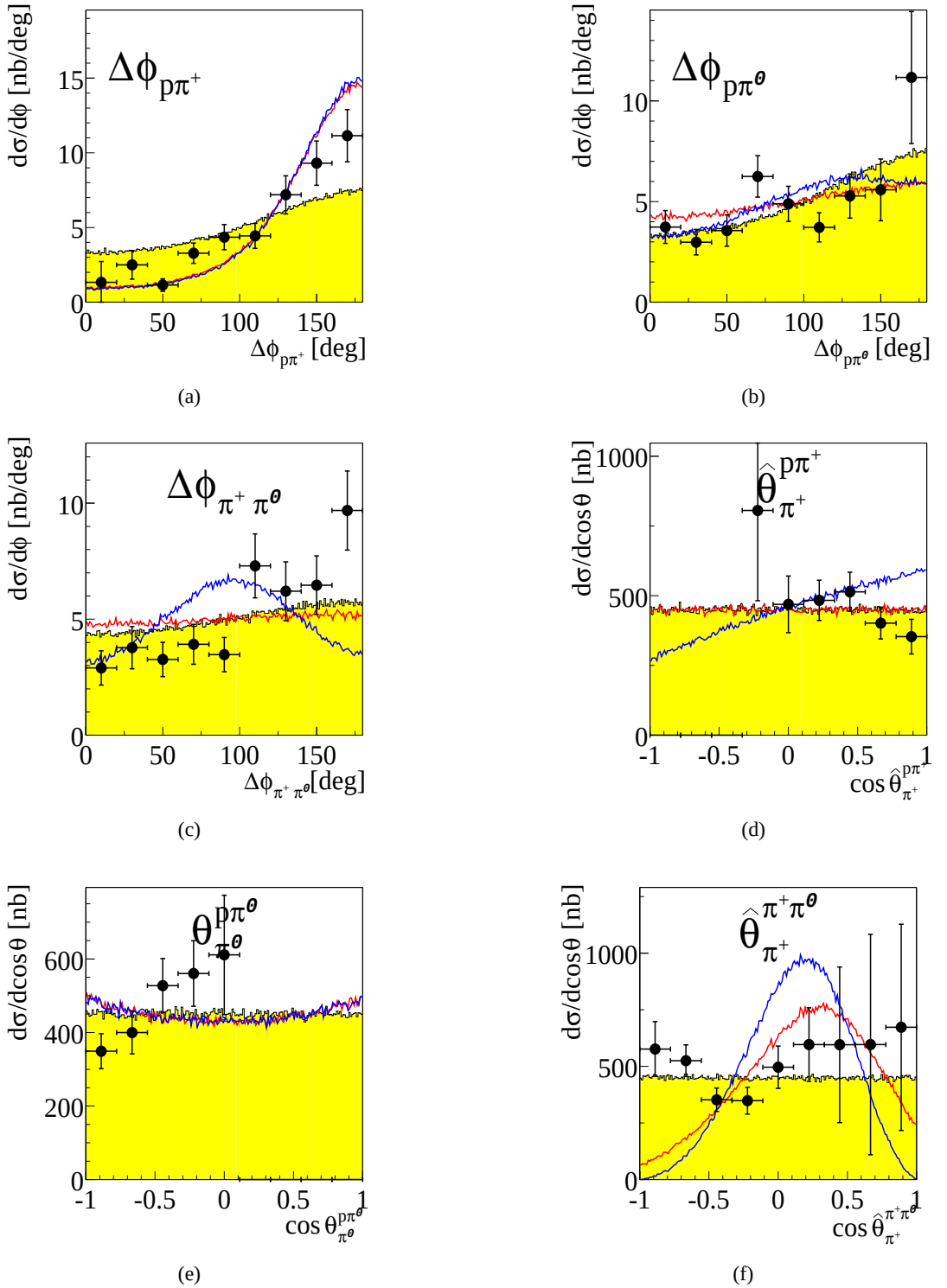

Figure 5.21.: Planarity ΔΦ distributions for (a) proton and π^+, (b) proton and π^0, (c) π^+ and π^0, angle distributions in subsystems between between track and sum vector for (d) π^+ in proton π^0 subsystem and (f) π^+ in $\pi^+\pi^0$ subsystem, (e) angle distribution between π^0 track in subsystem proton π^0 and z-axis

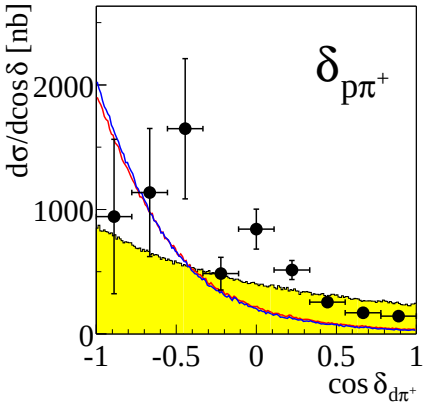

(a)

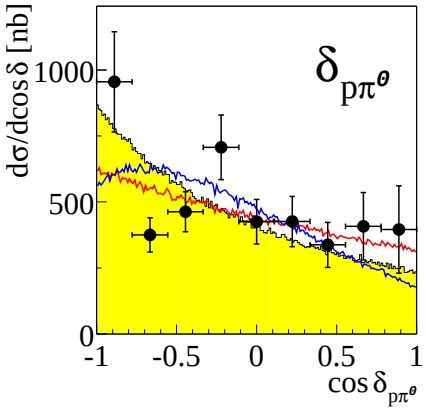

(b)

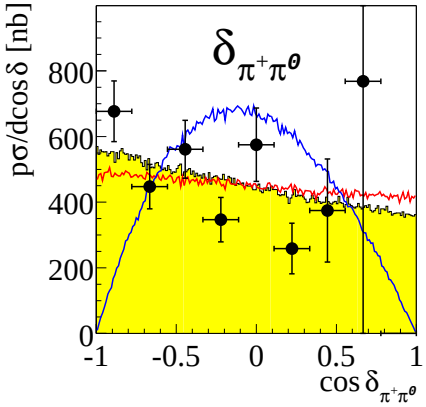

(c)

Figure 5.22.: Opening angle distributions between tracks for (a) proton and π^+, (b) proton and π^0 and (c) π^+ and π^0

5.5.2. Discussion of results for pn$\pi^+\pi^0$

As described in section 4.3.2 the selection of $pp \to pn\pi^+\pi^0$ events was made difficult by a large background. Therefore the Figures 5.19(c) and 5.19(d) are important, since they show a reasonable symmetric $\theta^{c.m.}$ distribution for p and π^0. In selections where background is known to be present (e.g. Fig. 4.13), $\theta_p^{c.m.}$ and $\theta_{\pi^0}^{c.m.}$ both show a falling slope from backward to forward angles. As such a slope cannot be excluded in Fig. 5.19(c) due to error bars, background cannot be completely excluded. But if there is a slope, it is much less steep than in the samples with known background. Therefore we conclude that the background contributes at most only a minor part of the selected data and the dominating part are real pn$\pi^+\pi^0$ events.

Originally it was assumed, that the $pp \to pn\pi^+\pi^0$ reaction has a similar mechanism as $pp \to d\pi^+\pi^0$. But this is proven wrong by data:

The spin flip term $\vec{\sigma} \cdot (\widehat{k_1} \times \widehat{k_2})$ would produce in the opening angle a sine modulated distribution as shown by the red curve in Fig. 5.22(c). But the data does not show such a behaviour.

Of the four invariant mass plots (Fig. 5.15(a), 5.15(b), 5.16(b) and 5.16(c)) , where a Δ should be visible according to the models only Fig. 5.15(a) shows some enhancement, but with very low statistics.

This does not necessarily mean that there is no Δ excitation. As visible in Fig. 5.15(a) there are acceptance problems at least for Δ^{++}. And just as the spin flip term has influence on the shape of the Δ peak - visible in the Figures as blue and red curves - a better description of the reaction mechanism could yield Δ peaks, which are not visible in these data. But the reaction mechanism, which proved to be valid for d$\pi^+\pi^0$, is not present in the pn$\pi^+\pi^0$ channel. Therefore efficiency and acceptance correction was done with a phase space assumption.

5.5.3. Total cross section

As in case of the $pp \to d\pi^+\pi^0$ channel the total cross section is derived by determining the cross section $pp \to pn\pi^+\pi^0$ relative to known $pp \to pp\pi^0$ cross section. The relative cross section is obtained by comparing the number of events, since for both reactions the same trigger is used.

Table 5.2 shows the event numbers for data, simulation and simulation through detector for the two reactions. The total number of events in all runs is calculated by (data*simulation/simulation through detector). The relative cross section $\sigma_{d\pi^+\pi^0}/\sigma_{pp\pi^0}$ is calculated by (calculated number of events d$\pi^+\pi^0$/calculated number of events ppπ^0). The total cross section is calculated by multiplying the relative cross section with 4.3 - 4.9 mb (Value from Ref. [9]).

As this selection is an extensive cut into available phase space, the cross section derived from this selection is very model dependent. Since the correct model is not known, the derived cross section should only be considered as a rough estimate. As a test for the model effect a model only with Δ-propagators was used. Using this model the cross section changes by 21%.

Therefore assuming a phase space like behavior the result of the total cross section for $pp \to pn\pi^+\pi^0$ is:

$\sigma_{pn\pi^+\pi^0}$ **= 0.33 $\pm$ 0.09 mb** , $\qquad E_{beam} = 1.1 GeV$

	$pn\pi^+\pi^0$	$pn\pi^+\pi^0$ $\Delta\Delta$	$pp\pi^0$ number of events
data	262	262	19110
model	1955802	1840034	1034259
model through detector	1044	802	2925
calculated number of events	490823	601108	6757158
$\sigma_{pn\pi^+\pi^0}/\sigma_{pp\pi^0}$	0.0726	0.0889	
$\sigma_{pn\pi^+\pi^0}$ μb	310-355	380-435	

Table 5.2.: Number of events in $pn\pi^+\pi^0$ and $pp\pi^0$ and approximate total cross section of $pp \rightarrow pn\pi^+\pi^0$

This cross section is in the range of previous bubble chamber measurements (Ref. [8]).

6. Conclusion and Outlook

The first exclusive measurements of the double-pionic fusion reaction to an isovector $\pi\pi$ channel with a beam energy of 1.1 GeV provide differential cross sections, which are in good agreement with a conventional t-channel $\Delta\Delta$ excitation in the intermediate state though small contributions from other processes can not be excluded.
As expected from the Bose symmetry of the $\pi\pi$ system, which prohibits relative s-waves between π^+ and π^0, the isovector $\pi^+\pi^0$ system in the $pp \to d\pi^+\pi^0$ channel shows no low invariant mass enhancement. This confirms, that the ABC effect is indeed a scalar-icoscalar effect. These results were published, see Ref. [30]. Since then a correction of the $pp \to pp\pi^0$ analysis led to a corrected cross section, which fits well into the observed energy dependence of the total cross section. This is described well by the t-channel $\Delta\Delta$ process including the isovector operators.

Further on this channel opens the possibility to predict the size of the conventional t-channel $\Delta\Delta$ contribution in $pn \to d\pi^+\pi^-$ and $pn \to d\pi^0\pi^0$, see Ref. [11].

The differential cross sections of the related non-fusion double-pionic reaction channel $pp \to pn\pi^+\pi^0$ measured at the same beam energy show that a different reaction mechanism is present in fusion and non-fusion processes. For the non-fusion channel a cross section has been determined.

In 2005 the WASA detector was moved from the Theodor-Svedberg-Lab in Uppsala to the Forschungszentrum Juelich and is meanwhile operating as an internal detector at the COSY facility. The channel $pp \to d\pi^+\pi^0$ is studied further with much improved statistics and at several different energies above, below and around the double Δ region. Further ongoing studies concern the energy dependence of the ABC effect in the double-pionic fusion reactions to ^3He (Ref. [28]) and ^4He (Ref. [29]).

A. Trigger lists

Trigger/scaler configuration list
Prescaled triggers

Location: WASA_COMMON_ROOT:[DOC.RUNS.TRIGGER]
Created KF 2003-03-26, updated 030605 Time/tape of validity:
030526, 21:45, run 67-75 , 1100 MeV, pp Runperiod: 540200

Prescaler number & trigger number & trigger matrix no.	Prescaler channel	NIM/ECL channel	Trigger definition	Ofline code	Prescale factor	Connected to DAQ *)	Scaler position in DAQ ***)	TDC position in DAQ ***)
Prescaler 1, NIM/ECL unit 3, 1-16, FB0 Scaler 16-31, FB0 TDC 48-63								
PT 0	0	1	fhds1	BF1			00616	00748
1	1	2	frha2delayed*ps2	#N/A			00617	00749
2	2	3	frha1	BF2	6000	X	00618	00750
3	3	4	fwc1	BF5			00619	00751
4	4	5	psf1	BC2			00620	00752
5	5	6	psc1	BC1			00621	00753
6	6	7	Vps	WC14			00622	00754
7	7	8	fhdw2	BF24			00623	00755
8	8	9	lpp	BL1	1	X	00624	00756
9	9	10	frha2	BF22	700	X	00625	00757
10	10	11	fwc2*frhe2	#N/A			00626	00758
11	11	12	Vfwc*Vfhds*frhe2*ps2	#N/A	3	X	00627	00759
		13	Gates				00628	00760
		14	Accepted triggers				00629	00761
		15	Triggers in				00630	00762
		16	100kHz				00631	00763
Prescaler 2, NIM/ECL unit 4, 1-16, FB1 Scaler 16-31, FB0 TDC 80-95								
12	0	1	se1n*Pfhdw2ps2	#N/A	1	S	10116	00780
13	1	2	fwc1*Vfwc2*fhds1*Vfhds2*frhe2*ps1	#N/A	54	X	10117	00781
14	2	3	fwc1*fhds1*frha1*ps3	#N/A	25	X	10118	00782
15	3	4	ps2	BC24			10119	00783
16	4	5	ps1	BC14	10000	X	10120	00784
17	5	6	psf1*psc1	#N/A	1500	X	10121	00785
18	6	7	ecf2*Pfhdw2ps2	#N/A	3	S	10122	00786
19	7	8	fhdw2*ps2	#N/A			10123	00787
20	8	9	ps2*frha2	#N/A	150		10124	00788
21	9	10	psc1*frha1	#N/A	2000	X	10125	00789
22	10	11	seccf2*Vpsd*Pwc2hds2rh2Vps	#N/A	1	S	10126	00790
23	11	12	fwc2*fhds2*frha2*ps2	#N/A	5	X	10127	00791
		13	2nd level in				10128	00792
		14	Accepted triggers				10129	00793
		15	1st level in				10130	00794
		16	100kHz				10131	00795
Prescaler 3, NIM/ECL unit 5, 1-16, FB2 Scaler 16-31, VME scaler 16-31								
24	0	1	ecf2*Vpsd*Pfhdw2Vps	#N/A	3	S	20316	00709
25	1	2	ec1*Pfhdw2re2ps2	#N/A			20317	00710
26	2	3	seccf1*Pwc1hds1rh1ps1	#N/A	1	S	20318	00711
27	3	4	ec1	BC11			20319	00712
28	4	5	ec1*Vpsd*Pfhdw2Vps	#N/A	2	S	20320	00713
29	5	6	ef1*Vpsd*Pfhdw2Vps	#N/A	1	S	20321	00714
30	6	7	seccf2*Pwc1hds1rh1ps1	#N/A	1	S	20322	00715
31	7	8	lpc	BL2	1	X	20323	
		9	Blocked FHDS				20324	
		10	Blocked 100kHz				20325	
		11	10kHz				20326	
		12	100Hz				20327	
		13	Ibeam				20328	
		14	Accepted triggers				20329	
		15	Pellet Dump				20330	
		16	100kHz				20331	

Trigger matrix, NIM/ECL unit 6, 1-4, FB2 Scaler 0-3, FB0 TDC 0-3

32		1	First level triggers				20300	00700
33		2	2Pretriggers				20301	00701
34		3	Second level triggers				20302	00702
35		4						

Prescaler 4, NIM/ECL unit 6, 5-16, FB2 Scaler 4-15, FB0 TDC 4-15

36	0	5	Pfhdw2rhb2ps2 = ps2*fhdw2*frhb2	P242	10		20304	00704
37	1	6	Pfhdw2re2ps2 = fhdw2*frhe2*ps2	P247	1		20305	00705
38	2	7	Pfhdw2ps2 = ps2*fhdw2	P241	6	P	20306	00706
39	3	8	Pfhdw2Vps = fhdw2*Vps	P051	4	P	20307	00707
40	4	9	Pwc2hds2rh2Vps = fwc2*fhds2*frha2*Vps	P061	1	P	20308	00708
41	5	10	Pwc1hds1rh1ps1 = fwc1*fhds1*frha1*ps1	P301	20	P	20303	00703
42	6	11	Pfwc1fhdw2ps2 = fwc1*fhdw2*ps2	P232	1			
43	7	12	Pfwc1frha2Vps = fwc1*frha2*Vps	P02	1			
44					1			

*) X primary trigger, S secondary trigger, P pretrigger
***) abbcc where a is crate no., b is slot no. and c is channel no.
****) 1MHz to scaler on this channel

Figure A.1.: List of triggers, only triggers with a S or X entrance in ”Connected to DAQ” were used for data taking, p marks a pretrigger, which only gave a signal for use in other triggers

B. Acknowledgments

My first and foremost thanks go to Prof. Heinz Clement for the invaluable advice he offered and the patience with which he supported my work.

Second for the work, but more heartfelt my thanks go to my wife Katharina Ehrhardt for all the love, encouragement, assistance and help she had even while working on her own Ph.D. Thesis.

Much thanks for answering both stupid and hopefully not so stupid questions to Mikhail Bashkanov, who was first target due to sharing the same room during the entire time.

Thanks also to Tatiana Skorodko, Evgeny Doroshkevich and Olena Khakimova for their welcome advice especially regarding the analysis software.

Thanks to Uppsala Wasa group for the help to understand the trigger system, the MDC and for the nice and fascinating stays at Uppsala.

To Annette Pricking, Elena Perez and the other colleagues at Physikalisches Institut Tuebingen for the great atmosphere there - barbecue season from March to October.

Prof. Gerhard Wagner I'd like to thank for his help he gave while finishing this thesis.

Special thanks go to my children Yannick, Chiara and Raphael for always exercising my skills in multi-tasking, going-with-little-sleep and withstand-stress and for all the fun. In this regards a big thank to my mother and my father, who always were ready to help, when the exercises offered by my children went to far.

Bibliography

[1] N.E. Booth, A. Abashian, K.M. Crowe, Phys. Rev. Lett. **7** (1961) 35;
N.E. Booth, A. Abashian, K.M. Crowe, Phys. Rev. Lett. **5** (1960) 258;
N.E. Booth, A. Abashian, K.M. Crowe, Phys. Rev. **C132** (1963) 2296ff.

[2] J. Banaigs, et al., Nucl. Phys. **B67** (1973) 1.

[3] See, e.g., R. Wurzinger, et al., Phys. Lett. **B445** (1999) 423; For a review see A. Codino, F. Plouin, LNS/Ph/94-06.

[4] F. Plouin et al., Observation of the ABC Effect in the reaction n + p ! d+(mm)0 with a 1.88 GeV/c Neutron Beam, Nucl. Phys. **A302**, 413 (1978)

[5] F. Plouin, P. Fleury, C. Wilkin, Phys. Rev. Lett. **65** (1990) 690.

[6] C.A. Mosbacher, F. Osterfeld, Double Δ (1232) excitation and the ABC effect in the reaction n + p $\rightarrow {}^2$H($\pi\pi$), nucl-th/9903064

[7] T. Risser, M.D. Shuster, Phys. Lett. **43B** (1973) 68.

[8] F. Shimizu, et al., Nucl. Phys. **A386** (1982) 571.

[9] J. Bystricky, et al., J. Physique **48** (1987) 1901, and references therein.

[10] M. Bashkanov, et al., Phys. Lett. **B637** (2006) 223, arXiv:nucl-ex/0508011.

[11] M. Bashkanov, et al., Phys. Rev. Lett. **102** (2009) 052301, arXiv:0806.4942 [nuclex].

[12] O. Khakimova, Ph.D. thesis, University of Tübingen, 2009.

[13] H. Clement, et al., Prog. Part. Nucl. Phys. **61** (2008) 276, arXiv:0712.4125 [nuclex].

[14] S. Keleta, et al., Nucl. Phys. **A825** (2009) 71.

[15] M. Bashkanov, et al., in: I. Tserruya, A. Gal, D. Ashery (Eds.), Proc. PANIC08, Elsevier, 2009, p. 239, arXiv:0906.2328 [nucl-ex].

[16] T. Skorodko, et al., Phys. Lett. **B6679** (2009) 30, arXiv:0906.3087 [nucl-ex].

[17] Bargholtz Chr., CELSIUS-WASA Collab., The WASA detector facility at CELSIUS, Nuclear Instruments and Methods in Physics Research Section A, 594 (2008) 3, 339-350

[18] M. Jacewicz, Measurements of the reaction $pp \to pp\pi^+\pi^-\pi^0$ with CELSIUS/WASA at 1.36 GeV, Ph.D. Thesis, Uppsala University, 2004.

[19] M. Bashkanov Double Pionic Fusion, Ph.D. Thesis, University of Tübingen, 2006.

[20] H. Pilkuhn, The interaction of hadrons (North-Holland Publishing Co., Amsterdam 1967)

[21] L. Alvarez-Ruso, Phys. Lett. **B452** (1999) 207; L. Alvarez-Ruso, PhD thesis, Univ. Valencia, 1999.

[22] L. Alvarez-Ruso, E. Oset, E. Hernandez, Nucl. Phys. **A633** (1998) 519 and priv. comm.

[23] S. Huber, J. Aichelin, Production of Δ- and N^*-resonances in the one-boson exchange model, Nucl. Phys. **A573** (1994) 587-625

[24] J.C. Anjos, D. Levy, A. Santoro, Nucl. Phys. **B67** (1973) 37.

[25] See, e.g., A. Gardestig, G. Fldt, C. Wilkin, Phys. Rev. **C59** (1999) 2608; A. Gardestig, G. Fldt, C. Wilkin, Phys. Lett. **B421** (1998) 41; C.A. Mosbacher, F. Osterfeld, arXiv:nucl-th/9903064.

[26] T. Skorodko, PhD thesis, University of Tübingen, 2009

[27] Chr. Bargholtz, et al., Nucl. Instr. Meth. **A594** (2008) 339.

[28] E. Perez, Ph.D. thesis, University of Tübingen, in preparation

[29] A. Pricking, Ph.D. thesis, University of Tübingen, in preparation

[30] F. Kren, et. al., Phys. Lett. **B684** (2010) 110-113

[31] T. Ericson, W. Weise, Pions and Nuclei (Clarendon Press, Oxford 1988)

List of Publications

Systematic Study of Two-Pion Production in NN Collisions – from Single-Baryon to Di-Baryon Excitations. By CELSIUS/WASA Collaboration (T. Skorodko et al.). Jan 2010. arXiv:1001.5446[nucl-ex]

Production of eta and 3 π mesons in the pd3 → HeX reaction at 1360 and 1450 MeV. K. Schoenning et al. Jan 2010. arXiv:1001.4604[nucl-ex]

The pd →He-3 $\eta\pi^0$ reaction at T_p = 1450 MeV. By CELSIUS/WASA Collaboration (K. Schonning et al.). Nov 2009. Published in Phys.Lett.B685:33-37,2010. arXiv:0911.1012[nucl-ex]

Exclusive Measurements of $pp \to d\pi^+\pi^0$: Double-Pionic Fusion without ABC Effect. By CELSIUS/WASA Collaboration (F. Kren et al.). Oct 2009. Published in Phys.Lett.B684:110-113,2010. arXiv:0910.0995[nucl-ex]

Two-Pion Production in Proton-Proton Collisions: Experimental Total Cross Sections and their Isospin Decomposition. T. Skorodko et al. Jun 2009. Published in Phys.Lett.B679:30-35,2009. arXiv:0906.3087[nucl-ex]

The $pp \to d\pi^+\pi^0$ reaction: A case of Delta Delta excitation without ABC-effect. By CELSIUS-WASA Collaboration (F. Kren et al.). 2009. Published in Int.J.Mod.Phys.A24:561-563,2009.

Isospin decomposition of $pp \to NN\pi\pi$ cross sections: Do we see a sign of Delta(1600) excitation in the n n $\pi^+\pi^+$ channel? By CELSIUS-WASA Collaboration (T. Skorodko et al.). 2009. Published in Int.J.Mod.Phys.A24:450-453,2009.

Eta production in proton-proton collisions at 72-MeV excess energy. By CELSIUS-WASA Collaboration (H. Pettersson et al.). 2009. Published in Int.J.Mod.Phys.A24:446-449,2009.

Exclusive measurement of two-pion production in the dd → He-4 ππ reaction. S. Keleta et al. Apr 2009. Published in Nucl.Phys.A825:71-90,2009. arXiv:0904.2699[nucl-ex]

Production of the omega meson in the pd → He-3 ω reaction at 1450-MeV and 1360-MeV. By CELSIUS/WASA Collaboration (K. Schonning et al.). Feb 2009. (Published Apr 2009). Published in Phys.Rev.C79:044002,2009. arXiv:0902.3905[nucl-ex]

Measurement of the $\eta - -- > 3\pi^0$ *Dalitz Plot Distribution with the WASA Detector at COSY.* By WASA-at-COSY Collaboration (C. Adolph et al.). Nov 2008. Published in Phys.Lett.B677:24-29,2009. arXiv:0811.2763[nucl-ex]

ABC effect: A signal of a quasibound Delta Delta system. By CELSIUS-WASA Collaboration (M. Bashkanov et al.). 2008. Published in Prog.Part.Nucl.Phys.61:304-305,2008.

Roper resonance: Its static and dynamic properties from single- and double-pion production. By CELSIUS-WASA Collaboration (T. Skorodko et al.). 2008. Published in Prog.Part.Nucl.Phys.61:168-169,2008.

Double-Pionic Fusion of Nuclear Systems and the ABC Effect: Aproaching a Puzzle by Exclusive and Kinematically Complete Measurements. M. Bashkanov et al. Jun 2008. (Published Feb 6, 2009). Published in Phys.Rev.Lett.102:052301,2009. arXiv:0806.4942[nucl-ex]

Polarisation of the omega meson in the $pd \to$ *He-3* ω *reaction at 1360 and 1450-MeV.* By CELSIUS/WASA Collaboration (K. Schonning et al.). Jun 2008. Published in Phys.Lett.B668:258-262,2008. arXiv:0806.2945[nucl-ex]

Excitation of the Roper resonance in single- and double-pion production in nucleon-nucleon collisions. T. Skorodko et al. 2008. Published in Eur.Phys.J.A35:317-319,2008.

The WASA Detector Facility at CELSIUS. By CELSIUS/WASA Collaboration (Chr. Bargholtz et al.). Mar 2008. Published in Nucl.Instrum.Meth.A594:339-350,2008. arXiv:0803.2657[nucl-ex]

Two-pion production in the Delta Delta region: Is the ABC-effect the result of a resonance in the p n ¡−¿ Delta Delta system? By CELSIUS-WASA Collaboration (M. Bashkanov et al.). 2007. Published in AIP Conf.Proc.950:256-258,2007.

Single- and Double-Pion Production in Nucleon Collisions on the Nucleon and on Nuclei – the ABC Effect and its Possible Origin in a Dibaryonic Resonance. By CELSIUS-WASA Collaboration (H. Clement et al.). Dec 2007. Published in Prog.Part.Nucl.Phys.61:276-282,2008. arXiv:0712.4125[nucl-ex]

Low-mass pi pi enhancement in baryonic pi pi production: ABC effect revised by exclusive measurements. By CELSIUS-WASA Collaboration (M. Bashkanov et al.). 2007. Published in Int.J.Mod.Phys.A22:625-628,2007.

Observation of the ABC effect in the first exclusive measurements of $pn \to d\pi^0\pi^0$. By CELSIUS-WASA Collaboration (O. Khakimova et al.). 2007. Published in Int.J.Mod.Phys.A22:617-620,2007.

π π *production in proton proton collisions.* By CELSIUS-WASA Collaboration (T. Skorodko et al.). 2007. Published in Int.J.Mod.Phys.A22:509,2007.

Large sigma channel low-mass enhancement in exclusively measured double pionic fusion to He-3. By CELSIUS-WASA Collaboration (M. Bashkanov et al.). 2006. Published in AIP Conf.Proc.842:440-442,2006. Also in *Santa Fe 2005, Particles and nuclei* 440-442

Two-pion production in nucleon-nucleon collisions and the ABC-effect: Approaching a puzzle by exclusive and kinematically complete measurements. T. Skorodko et al. Dec 2006. Published in *Yalta 2006, New trends in high-energy physics* 119-130 nucl-ex/0612016

Evidence for a 'narrow' roper resonance: The Breathing mode of the nucleon. H. Clement et al. Dec 2006. Published in *Yalta 2006, New trends in high-energy physics* 23-32 nucl-ex/0612015

Anisotropy in the pion angular distribution of the reaction $pp \to pp\pi^0$ *at 400-MeV.* P. Thorngren Engblom et al. Sep 2006. (Published Sep 2006). Published in Phys.Rev.C76:011602,2007. nucl-ex/0609003

On the pi pi production in free and in-medium N N collisions: sigma-channel low-mass enhancement and π^0 π^0 */ pi*$^+$ *pi*$^-$ *asymmetry.* By CELSIUS/WASA Collaboration (M. Bashkanov et al.). 2005. Published in Acta Phys.Slov.56:285-297,2006.

Double-pionic fusion to He-3: ABC effect revised. By CELSIUS-WASA Collaboration (M. Bashkanov et al.). May 2005. Published in *Bonn 2005, Nuclear physics at storage rings* 129-132

Two-pion production, gamma gamma line and aspects of sigma meson, Bose-Einstein correlations and isospin breaking. By CELSIUS-WASA Collaboration (H. Clement et al.). 2005. Published in Int.J.Mod.Phys.A20:1747-1752,2005.

Proposal for the wide angle shower apparatus (WASA) at COSY-Julich: WASA at COSY. By WASA-at-COSY Collaboration (H.-H. Adam et al.). Oct 2004. nucl-ex/0411038